Available online at www.sciencedirect.com
ScienceDirect
GEOBIOS
Geobios 39 (2006) 563–584
http://france.elsevier.com/direct/GEOBIO/

Original article

An almost complete skeleton of *Metailurus parvulus* (Carnivora, Felidae) from the late Miocene of Kerassia (Northern Euboea, Greece)

Un squelette presque complet de *Metailurus parvulus* (Carnivora, Felidae) du Miocène supérieur de Kerassia (Eubée du Nord, Grèce)

Socrates J. Roussiakis [a,*], George E. Theodorou [a], George Iliopoulos [b]

[a] *Faculty of Geology and Geoenvironment Department of Historical Geology and Palaeontology, National and Kapodistrian University of Athens, Panepistimiopolis, 15784 Athens, Greece*
[b] *Department of Geology, University of Leicester, LE1 7RH, Leicester, UK*

Received 17 December 2004; accepted 11 April 2005
Available online 28 July 2006

Abstract

We describe a partial skeleton of *Metailurus parvulus* from the Turolian site of Kerassia 1 (Northern Euboea, Greece). The material, which consists of a mandible, the anterior and posterior limb-bone elements, some sternal bones and some vertebrae, is the most complete known of this species. The dental material is compared to specimens from Pikermi and Chomateri (Greece), and China. The limb-bones available offer us the possibility to discuss the status of some previously described specimens from Pikermi. The limb proportions indicate that *M. parvulus* had elongated posterior limbs relative to the anterior ones, which reflects developed jumping skills. *M. parvulus* had moderately developed cursorial abilities, intermediate between open and closed habitat felids, and probably frequented primarily relatively open woodlands.

Résumé

Nous décrivons ici un squelette presque complet de *Metailurus parvulus* qui provient de la localité turolienne de Kerassia 1 (Eubée du Nord, Grèce). Le matériel, constitué d'une mandibule, des segments des membres antérieurs et postérieurs, et des portions de la colonne vertébrale et du sternum, est le plus complet connu de cette espèce. La denture est comparée aux pièces de Pikermi et Chomateri (Grèce), et de Chine. Les os des membres disponibles nous offrent la possibilité de discuter l'état de quelques pièces déjà décrites provenant de Pikermi. Les proportions des membres de *M. parvulus* indiquent que le membre postérieur était plus long que le membre antérieur, ce qui montre que *M. parvulus* était capable de bonds puissants. Ses adaptations à la course étaient médiocrement développées et le classent dans une situation intermédiaire entre les félidés de terrain ouvert et ceux des forêts. *M. parvulus* fréquentait probablement des régions légèrement boisées.

Keywords: *Metailurus*; Felidae; Carnivora; Euboea; Greece, Late Miocene; Palaeoecology

Mots clés : *Metailurus* ; Felidae ; Carnivora ; Eubée ; Grèce, Miocène supérieur ; Paléoécologie

* Corresponding author.
E-mail address: srousiak@geol.uoa.gr (S.J. Roussiakis).

0016-6995/$ - see front matter © 2006 Elsevier SAS. All rights reserved.
doi:10.1016/j.geobios.2005.04.002

1. Introduction

In 1992, the University of Athens started systematic excavations near the village of Kerassia, Northern Euboea. So far, seven fossiliferous sites have been located. Three of them (Kerassia 1, Kerassia 3 and Kerassia 4) are very rich in fossils. These sites are located across a road-site cut. They have been grouped into two fossiliferous levels: a lower one and an upper one. The Kerassia 1 (K1) site belongs to the upper fossiliferous level and is relatively younger stratigraphically than the sites Kerassia 2 (K2), Kerassia 3 (K3) and Kerassia 4 (K4) which belong to the lower fossiliferous level (Theodorou et al., 2001, 2003).

The excavations carried out until 2000 have shown that the mammalian fauna of the K1 site includes *Microstonyx major erymanthius*, *Palaeotragus rouenii*, *Helladotherium duvernoyi*, *Samotherium major*, *Tragoportax* cf. *amalthea*, *Gazella* sp., *Hipparion* sp., *Ancylotherium* sp., *Orycteropus* sp., *Metailurus* cf. *parvulus*, and possibly *Adcrocuta eximia* and *Choerolophodon* sp. (Roussiakis and Theodorou, 2003; Theodorou et al., 2003; Iliopoulos, 2003). The available up to now data indicate that a Middle Turolian (MN12) age is plausible for the Kerassia 1 site.

In 2001, the excavations in K1 revealed a significant part of a *M. parvulus* skeleton (Fig. 1). The material includes a mandible, most of the limb-bone elements, some cervical and thoracic vertebrae, and some ribs. The skull, the right humerus, most of the right hind limb-bones, the lumbar and caudal vertebrae, the sacrum, and the pelvis are missing. Most of the bones preserved were found articulated or associated, such as the left humerus and its corresponding zygopodium and autopodium elements. However, the humerus was rotated around its axis; thus the anconeal process of the ulna was not facing the olecranon fossa but the coronoid fossa of the humerus. The right radius, ulna and autopodium were mostly articulated, which is also the case with the left tibia, fibula and autopodium. However, the left femur was found about 30 cm away from its corresponding zygopodium joint. The same is true for the left scapula, which was found distal to the left manus and not, as expected, close to the proximal humerus head. The atlas and axis were disarticulated, but in contact with each other. Near these were the remaining cervical vertebrae and some sternal bones. The thoracic vertebrae were not in articulation except from some fragmentary centra. The mandible was found preserved close to the left scapula.

The recovered skeletal elements of *M. parvulus* were found at the top of the bone accumulation and occupied an area of approximately half a square metre. Accompanying it, some scarce *Hipparion* remains were found. The bones have perfectly preserved articular surfaces, and no signs of erosion. The stylopodium and zygopodium elements present longitudinal weathering cracks, indicating that these limb-bone elements were exposed on the surface for a significant period of time (Behrensmeyer, 1978). The fact that the *M. parvulus* remains were found either articulated or associated in such a small area, and even the presence of some light elements such as the ribs, indicate that the *M. parvulus* carcass was complete or almost complete at the time of transportation and the bone elements became disarticulated after its final deposition. The observed slight displacement of some limb-bone elements was probably due either to calm water movement or trampling. Most likely, the reason for the absence of some skeletal elements is that the local road was cut through the bone accumulation.

2. Material and methods

Dental and mandibular measurements follow the method of Werdelin and Solounias (1991). The methodology followed for each bone is given in the corresponding table of measurements. Even though many bones from the left and right side of the body are present, in some cases (carpalia, metapodials, phalanges) only the measurements of the better preserved speci-

Fig. 1. The skeleton of *M. parvulus* from the late Miocene of Kerassia 1.
Fig. 1. Le squelette de *M. parvulus* du Miocène supérieur de Kerassia 1.

mens are given. All measurements are given in mm with an accuracy of one decimal digit. Whenever we include bibliographic metric data we retain the original accuracy. Slightly inaccurate measurements are given in parentheses, or with the sign "+" in case of slightly broken specimens. Some rib fragments as well as sesamoid bones found are not included in this study. The terminology applied in the description of the anatomical characters is generally that of Jayne (1898), but the terminology used by other authors (Reighard and Jennings, 1901; Evans and Christensen, 1979) has also been taken into consideration. All the material is temporarily stored in the Athens Museum of Palaeontology and Geology. In the future, this material will be exhibited in a new museum planned in Kerassia by the local prefecture.

2.1. Material

Right astragalus (K1/105); distal metapodial part, right Mt III? (K1/106); 6th cervical vertebra (K1/195); atlas (K1/196); axis (K1/197); 4th cervical vertebra (K1/198); right scapula (K1/200); left femur (K1/201); left humerus (K1/202); left radius (K1/203); left ulna (K1/204); right patella (K1/205); thoracic vertebra (K1/206); 5th cervical vertebra (K1/207); right ulna (K1/208); right radius (K1/209/1); right scapholunar (K1/209/2); right cuneiform (K1/209/3); right pisiform (K1/209/4); right trapezium (K1/209/5); right trapezoid (K1/209/6); right unciform (K1/209/7); Ph 1, right manus, dig. I (K1/209/8); right Mc III (K1/209/9); Ph 1, right manus, dig. III (K1/209/10); Ph 2, right manus, dig. III (K1/209/11); right Mc II (K1/209/12); Ph 1, right manus, dig. II (K1/209/13); Ph 2, right manus, dig. II (K1/209/14); Ph 3, fragmentary, right manus, dig. II (K1/209/15); right Mc V, proximal part (K1/209/16); right Mc IV, proximal part (K1/209/17); right Mc IV, distal part (K1/209/18); right Mc I (K1/209/19); Ph 1, right manus, dig. V (K1/209/20); Ph 2, right manus, dig. V (K1/209/21); Ph 1, right manus, dig. IV (K1/209/22); Ph 2, right manus, dig. IV (K1/209/23); right mandible (K1/210); right Mt III, proximal part (K1/211); left scapula, fragmentary (K1/212); thoracic vertebra (K1/216); Ph 1, right pes, dig. III (K1/217); right Mt II (K1/251/1); Ph 1, right pes, dig. Mt II (K1/251/2); right mesocuneiform (K1/251/3); right Mt I (K1/251/4); left calcaneum (K1/252/1); left astragalus (K1/252/2); left navicular (K1/252/3); left cuboid (K1252/4); left mesocuneiform (K1/252/5); left entocuneiform (K1/252/6); left ectocuneiform (K1/252/7); left Mt III (K1/252/8); Ph 1, left pes, dig. III (K1/252/9); left Mt IV (K1/252/12); Ph 1, left pes, dig. IV (K1/252/13); Ph 2, left pes, dig. Mt IV (K1/252/16); Ph 3, left pes, dig. Mt IV (K1/252/17); left Mt II (K1/252/18); Ph 1, left pes, dig. Mt II (K1/252/19); Ph 2, left pes, dig. II (K1/252/20); Ph 3, left pes, dig. II (K1/252/21); left Mt V (K1/252/22); Ph 1, left pes, dig. V (K1/252/23); Ph 2, left pes, dig. V (K1/252/24); Ph 3, fragmentary, left pes, dig. V (K1/252/25); left tibia (K1/252/26); left fibula (K1/252/27); sternal bone, 253/1; sternal bone, 253/1; left scapholunar (K1/258/1); left cuneiform (K1/258/2); left pisiform (K1/258/3); left trapezium (K1/258/4); left trapezoid (K1/258/5); left magnum (K1/258/6); left unciform (K1/258/7); left radial sesamoid (K1/258/8); left Mc I (K1/258/9); left Mc II (K1/258/10); left Mc III (K1/258/11); left Mc IV (K1/258/12); left Mc V (K1/258/13); Ph 1, left manus, dig. I (K1/258/14); Ph 1, left manus, dig. III (K1/258/15); Ph 2, left manus, dig. III (K1/258/16); Ph 3, left manus, dig. III (K1/258/17); Ph 1, left manus, dig. II (K1/258/18); Ph 2, left manus, dig. II (K1/258/19); Ph 1, left manus, dig. IV (K1/258/21); Ph 2, left manus, dig. IV (K1/258/22); Ph 1, left manus, dig. V (K1/259/1); Ph 2, left manus, dig. V (K1/259/2); thoracic vertebra (K1/261); thoracic vertebra (K1/264); 3rd cervical vertebra (K1/265/1); first sternal bone (manubrium) (K1/265/2); thoracic vertebra (K1/268).

2.2. Abbreviations

AMPG, Athens Museum of Palaeontology and Geology, National and Kapodistrian University of Athens; MNHNP, Muséum national d'Histoire naturelle de Paris; NHML, Natural History Museum of London.

3. Palaeontology

Order CARNIVORA Bowdich, 1821
Family FELIDAE Fischer, 1817
Genus ***Metailurus*** Zdansky, 1924
Metailurus parvulus (Hensel, 1862)

3.1. Description

3.1.1. Mandible and dentition (Fig. 2 and Table 1)

The described mandible (K1/210) is similar to a mandibular specimen (K1/18) found earlier in the same locality. The latter

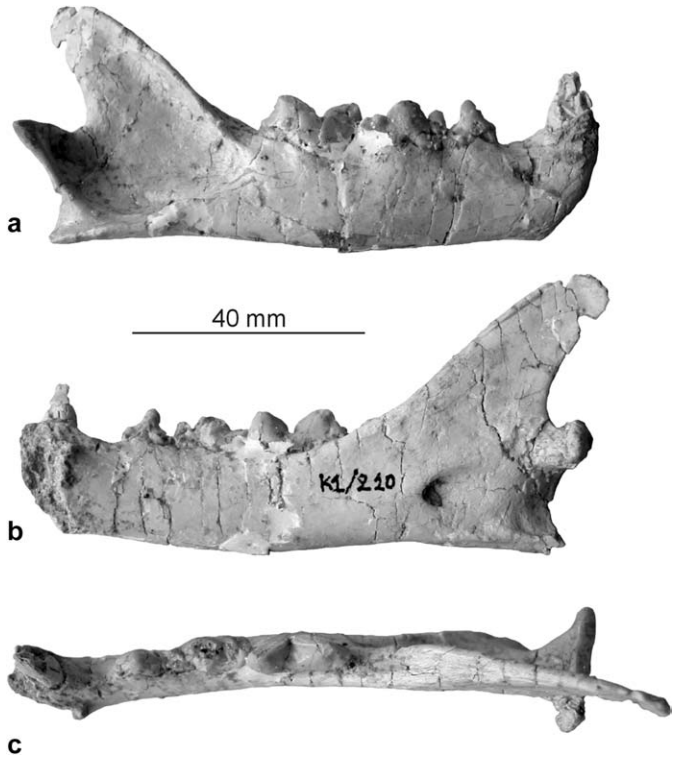

Fig. 2. Right mandible (K1/210): **a**) labial view **b**) lingual view **c**) occlusal view. Scale bar 40 mm.
Fig. 2. Mandibule droite (K1/210): **a**) vue labiale **b**) vue linguale **c**) vue occlusale. Échelle graphique 40 mm.

Table 1
Measurements of the mandibles and the lower teeth of *M. parvulus* from Kerassia 1, Pikermi, Chomateri, and China. (**1**) according to Weithofer (1888) and Thenius (1951); (**2**) according to Thenius (1951); (**3**) according to Zdansky (1924)
Tableau 1
Dimensions de la mandibule et de la denture inférieure de *M. parvulus* de Kerassia 1, Pikermi, Chomateri et Chine

	K1/210	K1/Δ18			PG 01/103	Unnumbered	
	Kerassia 1	Kerassia 1	Pikermi (**1**)	Pikermi (**2**)	Pikermi	Chomateri	China (**3**)
LC_i	(8.7)	(7.8)	9.1	–	8.1	8.3	8.8–9.6 ($n = 5$)
WC_i	(6.4)	(5.8)	6.6	–	5.7	6.0	6.3–(7.4) ($n = 5$)
diastema C_i–P_3	(8.8)	8.5	(7.2)	9.2	8.9	8.6	6.8–(11.0) ($n = 5$)
LP_3	(9.4)	(9.4)	–	10.3	9.7	9.9	9.9–10.7 ($n = 3$)
WP_3	(4.7)	(4.6)	–	5.1	4.9	5.1	5.1–5.3 ($n = 3$)
LP_4	14.3	(13.3)	15.0	14.4	14.2	13.9	14.5–15.4 ($n = 4$)
WP_4	(6.3)	6.0	6.5	5.9	5.7	5.8	6.1–6.9 ($n = 4$)
LM_1	17.3	–	17.8	17.2	17.3	17.1	16.7–18.1 ($n = 4$)
WM_1	7.1	–	7.0	6.9	6.9	7.0	6.9–7.8 ($n = 4$)
C_i–M_1	57.0	–	59.0	–	56.9	56.3	–
$LP_3 + LP_4 + LM_1$	(41.0)	–	–	41.9	41.2	40.9	41.4–44.2 ($n = 3$)
C_i–cond	99.3	–	–	–	–	101.2	–
Hdia	(17.0)	(17.5)	–	–	18.8	18.9	–
$HbehM_1$	19.4	–	–	–	20.1	19.4	–
HPC	(49.8)	–	–	–	–	–	–
Cond-ang	22.6	–	–	–	–	22.0	–
$(WC_i/LC_i) \times 100$	73.6	(74.4)	72.5	–	70.4	72.3	69.2–(77.1) ($n = 5$)
$(WP_3/LP_3) \times 100$	50.0	(48.9)	–	49.5	50.5	51.5	48.6–53.5 ($n = 3$)
$(WP_4/LP_4) \times 100$	(44.1)	(45.1)	43.3	41.0	40.1	41.7	42.1–45.4 ($n = 4$)
$(WM_1/LM_1) \times 100$	41.0	–	39.3	40.1	39.9	40.9	39.8–45.1 ($n = 4$)
$(LP_3/LP_4) \times 100$	(65.7)	(70.7)	–	71.5	68.3	71.2	68.3–70.3 ($n = 3$)
$(LP_3/LM_1) \times 100$	(54.3)	–	–	59.9	56.1	57.9	54.7–61.1 ($n = 3$)
$(LP_4/LM_1) \times 100$	82.7	–	84.3	83.7	82.1	81.3	80.1–86.8 ($n = 3$)
$(LM_1/LP_3 + LP_4) \times 100$	(73.0)	–	–	69.6	72.4	71.8	67.6–74.2 ($n = 3$)
$(C_i$–$P_3/LP_3) \times 100$	(93.6)	(90.4)	–	89.3	91.8	86.9	63.6–(84.8) ($n = 3$)
$(C_i$–$P_3/LM_1) \times 100$	(50.9)	–	(40.4)	53.5	51.4	50.3	37.6–(63.6) ($n = 4$)
$(C_i - P_3/LP_3 + LP_4 + LM_1) \times 100$	(21.5)	–	–	22.0	21.6	21.0	15.4–19.8 ($n = 3$)
$(LP_3 + LP_4 + LM_1/C_i - M_1) \times 100$	(71.9)	–	–	–	72.4	72.6	–

lacked the carnassial and was attributed to *Metailurus* cf. *parvulus* (Roussiakis and Theodorou, 2003). In the new mandible the canine and the cheek teeth are preserved, but the state of preservation is not very good. The canine is fragmentary and almost no enamel is preserved. The P_3 is damaged posteriorly, and the main cusp and mesolingual part of the P_4 are broken. The lower carnassial is well preserved but its protoconid and paraconid are much worn.

The mandibular ramus is slightly deeper behind the M_1 than in front of the P_3 and its ventral border is slightly convex below the cheek teeth. The ventrolateral angle of the symphysis appears gently curved in anterior and buccal view. There are two mental foramina: a large one under the middle of the postcanine diastema, and a very small one under the posterior border of the P_3. The anterior border of the masseteric fossa is below and slightly behind the posterior limit of the carnassial. The coronoid process extends posteriorly slightly more than the mandibular condyle. The angular process is broken. On its lingual side there is a crest that extends anteriorly almost to the level of the mandibular foramen that opens about 12 mm behind the M_1. The canine is not well preserved. The postcanine diastema is slightly smaller than the P_3 length, and shows no trace of a P_2. The P_3 has no anterior accessory cusp. Its posterior part is poorly preserved, but it probably had a small accessory cusp. The P_4 has two accessory cusps, and a slightly elevated posterior cingulum. The M_1 has a small talonid and a tiny metaconid.

3.1.2. Vertebral column, sternum

From the thoracic region five almost complete thoracic vertebrae, the fragmentary centra of three more vertebrae, and three sternal bones are preserved. The seventh cervical vertebra, the lumbar and caudal vertebrae, the sacrum and the pelvis are missing. Some ribs were also found. Unfortunately, it was not possible to extract them from the sediment in good condition. Thus they are not included in this study.

3.1.2.1. Atlas (Fig. 3(1) and Table 2). The transverse processes have rounded tips that do not extend much caudally, as they do for example in *Homotherium* (Ballesio, 1963: Fig. 16; Galobart et al., 2003). In lateral view, the transverse processes slope caudally and downwards. Their dorsal surface is slightly convex cranially, but concave caudally. The dorsal tubercle for the origin of the rectus capitis dorsalis minor muscle is well marked. The ventral tubercle for the attachment of the longus colli muscle is weak. The dorsoventral diameter of the neural canal (18.1 mm) is practically similar to the transverse diameter (18.6 mm). The facets of the cephalic articular processes

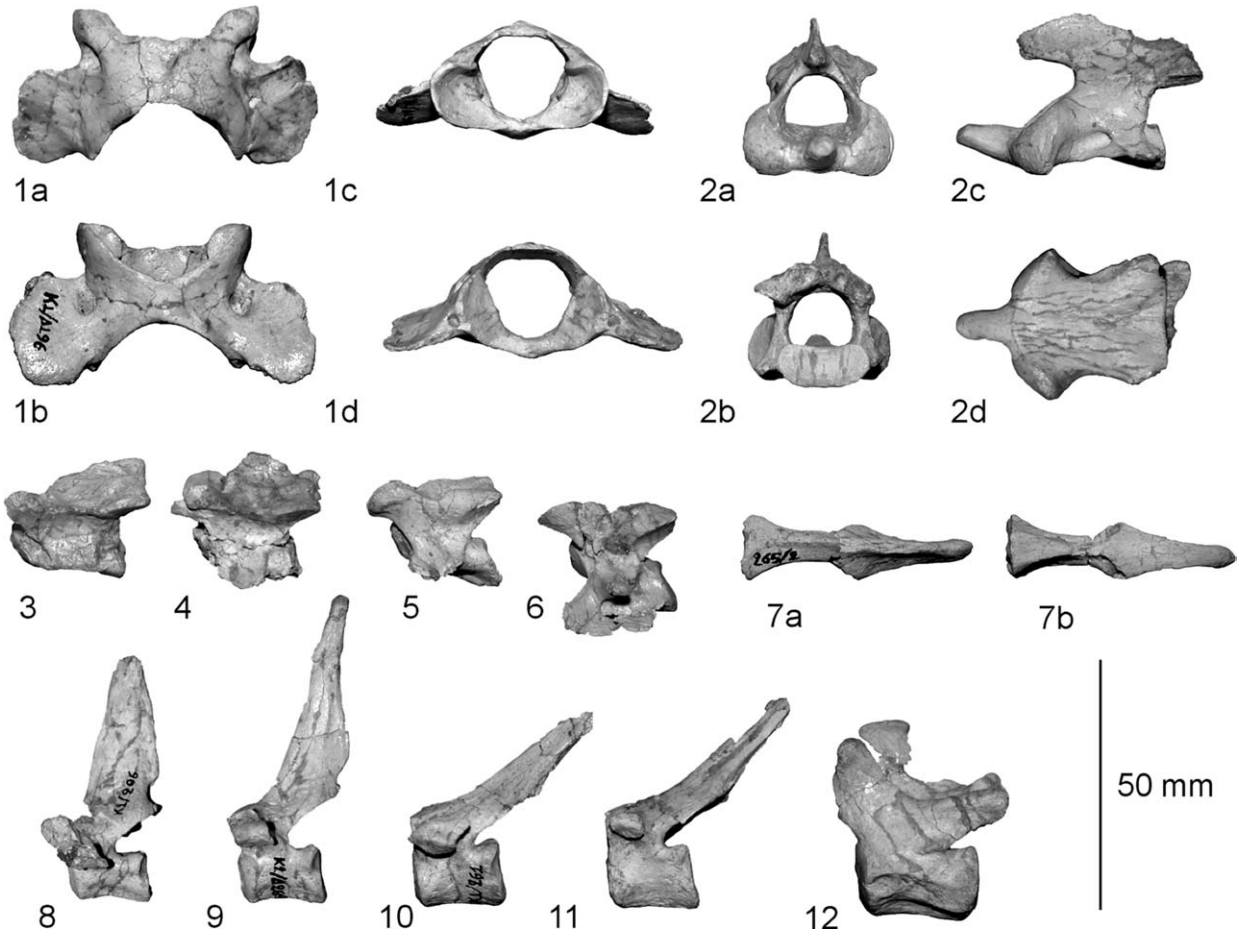

Fig. 3. **1**. Atlas (K1/196): **a**) dorsal view **b**) ventral view **c**) cranial view **d**) caudal view. **2**. Axis (K1/197): **a**) cranial view **b**) caudal view **c**) left lateral view **d**) ventral view. **3–6**. From left to right, 3rd (K1/265/1), 4th (K1/198), 5th (K1/207, inversed), and 6th (K1/195) cervical vertebra: left lateral view. **7**. Manubrium (K1/265/2): **a**) ventral view **b**) dorsal view. **8–12**. Thoracic vertebrae (from left to right K1/206, K1/264, K1/261, K1/268, K1/216): left lateral view. Scale bar 50 mm.
Fig. 3. **1**. Atlas (K1/196): **a**) vue dorsale **b**) vue ventrale **c**) vue craniale **d**) vue caudale. **2**. Axis (K1/197): **a**) vue craniale **b**) vue caudale **c**) vue latérale gauche **d**) vue ventrale. **3–6**. De gauche à droite, troisième (K1/265/1), quatrième (K1/198), cinquième (K1/207, inversée), et sixième (K1/195) vertèbre cervicale: vue latérale gauche. **7**. Manubrium (K1/265/2): **a**) vue ventrale **b**) vue dorsale. **8–12**. Vertèbres thoraciques (de gauche à droite K1/206, K1/264, K1/261, K1/268, K1/216): vue latérale gauche. Échelle graphique 50 mm.

Table 2
Measurements of the atlas of *M. parvulus* from Kerassia 1
Tableau 2
Dimensions de l'atlas de *M. parvulus* de Kerassia 1

	K1/196
Greatest width across the transverse processes	60.7
Width across the cephalic articular processes	35.7
Width at the articular surfaces for the epistropheus	29.5
Greatest craniocaudal diameter	35.0
Craniocaudal articular diameter	30.6
Sagittal craniocaudal diameter of the dorsal arc	(12.0)
Sagittal craniocaudal diameter of the ventral arc	(9.0)
Greatest dorsoventral height	24.5

are concave and overhanging dorsally. Their dorsal margin lies well below the dorsal margin of the neural arch. The tubercle for the transverse ligament is well developed, and the depression ventrally of this is especially marked. The *M. parvulus* atlas appears very similar in dimensions to a specimen from China referred to *Metailurus minor* by Zdansky (1924: Fig. 20), whereas the atlas of "*Metailurus anceps*" from Hadjidimovo-1 is larger and lacks the dorsal tubercle (Kovatchev, 2001).

3.1.2.2. Axis (Fig. 3(2) and Table 3). The neural spine, the transverse processes, and the right caudal articular process are partly broken. In ventral view, the cephalic articular processes lie at a very wide angle to each other, wider than in *Homotherium* from Senèze (Ballesio, 1963: Fig. 17b), and more similar to "*M. anceps*" (Kovatchev, 2001: Pl. 2, Fig. 1a) and *Homotherium serum* (Rawn-Schatzinger, 1992: Fig. 6). The caudal articular processes overhang the body, are subtriangular in shape, and face ventrally and slightly laterally. In ventral view, the body seems almost square, and has a strong constriction at its mid-length. Its length (excluding the odontoid process) is slightly larger than its width. The ventral keel is flanked by excavations for the longus colli muscle. The caudal articular surface of the body is transversely elongated. The axis of *M. parvulus* is much smaller than the "*M. anceps*" axis from Hadjidimovo-1 (Kovatchev, 2001). The latter approximates in size the specimen from Pikermi ("*Felis* sp.") figured by

Table 3
Measurements of the axis of *M. parvulus* from Kerassia 1
Tableau 3
Dimensions de l'axis de *M. parvulus* de Kerassia 1

	K1/197
Length of centrum and odontoid process	41.7
Length of the centrum	31.3
Width of the centrum across the cephalic articular surfaces	30.2
Height of the centrum at the cephalic articular surfaces	15.0
Width of the centrum at the caudal articular surface	18.9
Height of the centrum at the caudal articular surface	8.6
Width at the caudal articular processes	(27.0)
Transverse diameter of the odontoid process at its base	7.1

Weithofer (1888: Pl. 12, Fig. 3). Nevertheless, in "*Felis* sp." axis the posterior border of the cephalic articular processes appears almost vertical to the body of the vertebra in lateral view, as is the case in *Homotherium* from Senèze (Ballesio, 1963: Fig. 17a), whereas in *M. parvulus* it is oblique.

3.1.2.3. Posterior cervical vertebrae (Fig. 3(3–6) and Table 4). Since all available posterior cervical vertebrae have arterial canals but lack costal facets, it seems that the 7th cervical vertebra has not been found. However, the arterial canal is sometimes present in the 7th cervical vertebra of *Smilodon* and *Homotherium* (Antón and Galobart, 1999). The dorsal arch is not adequately preserved, except on the 3rd (K1/265/1; Fig. 3(3)) and 4th cervical vertebrae (K1/198; Fig. 3(4)). The hyperapophyses are preserved only on the 3rd and 4th cervical vertebrae. They are not especially developed, and are more widely separated on the 3rd cervical vertebra. On the 6th cervical vertebrae (K1/195; Fig. 3(6)) the dorsal portion of the transverse process (transverse element) is long and slender, almost perpendicular to the sagittal plane of the vertebra. This vertebra is not well preserved and it is not clear whether the ventral portion of the transverse process (costal element) is notched and divided into cephalic and caudal parts. All vertebrae have pronounced ventral keels flanked laterally by depressions. These characters are more pronounced on the 5th cervical vertebra (K1/207; Fig. 3(5)). The bodies have rectangular cranial articular surfaces that are transversely elongated, especially on the 3rd cervical vertebra. The caudal articular surfaces are more ovoid in shape.

Table 4
Measurements of the cervical vertebrae of *M. parvulus* from Kerassia 1
Tableau 4
Dimensions des vertèbres cervicales de *M. parvulus* de Kerassia 1

	C3 (K1/265/1)	C4 (K1/198)	C5 (K1/207)	C6 (K1/195)
Length of the centrum	23.2	(22.5)	23.3	24.4
Transverse diameter of the centrum, cranially	16.3	15.8	15.3	14.7
Height of the centrum, cranially	9.6	(10.3)	10.5	7.6
Transverse diameter of the centrum, caudally	17.3	(17.2)	15.8	15.9
Height of the centrum, caudally	8.3	–	10.1	11.2
Width at the cephalic articular processes	–	30.7	30.6	–
Width at the caudal articular processes	(27.7)	32.1	–	–

3.1.2.4. Thoracic vertebrae (Fig. 3(8–12) and Table 5). The thoracic vertebrae K1/206, K1/261, K1/264 and K1/268 belong to the prediaphragmatic region. K1/206 (Fig. 3(8)) has prezygapophyses, but lacks distinct postzygapophyses. There is also a concave area on the dorsal surface between the tip of the transverse process and the cephalic articular process. The prezygapophysial facets are of the radial type, whereas the postzygapophysial facets are of the tangential type (sensu Lessertisseur and Saban, 1967). The neural spine has the smallest caudal inclination of the available thoracic vertebrae, but it is not completely preserved. The characters of K1/206 indicate that it belongs to the cranial portion of the thoracic series and could correspond to the 2nd thoracic vertebra. The thoracic vertebrae K1/264 (Fig. 3(9)), K1/261 (Fig. 3(10)) and K1/268 (Fig. 3(11)) show tangential prezygapophysial and postzygapophysial facets and lack prominent prezygapophyses and postzygapophyses. The neural spine of K1/264 is completely preserved and its tip has a rounded tubercle. The large size and small caudal inclination of its neural spine indicate that K1/264 occupies a relatively cranial position. K1/261 and K1/268 have shorter neural spines with larger caudal inclinations and they could have a relatively caudal position. The thoracic vertebra K1/216 (Fig. 3(12)) has prezygapophysial and postzygapophysial facets of the radial type, and belongs to the caudalmost part of the thoracic series. It lacks true transverse processes for articulation with the ribs, and the ribs articulate to rounded fossae located close to the cranial end of each side of the body. The anapophyses are level with the postzygapophyses, overhang the caudal articular surface of the body, and have rounded tips. The neural spine slightly surpasses the metapophyses in height and is cranially inclined to a small degree. The tip of the neural spine is a craniocaudally elongated tubercle, slender anteriorly and thicker posteriorly. The body is much larger than that of the other vertebrae. Ventrally it has a strong ridge at the midline, and two shorter ridges on either side confined to the posterior half of the body. The characters of K1/216 and the small cranial inclination of its neural spine indicate that it could be the 12th or 13th thoracic vertebra.

3.1.2.5. Sternal bones (Fig. 3(7)). The first sternal bone or manubrium (K1/265/2) measures 46.2 mm in length. Its maximum width (at its caudal part) measures 12.8 mm and the width at the costal tubercles is 11.0 mm. The costal tubercles lie somewhat anteriorly relative to the anteroposterior middle of the bone. The caudal articular surface has the form of a trapezium with the ventral side larger. The ventral keel is strong. Two more sternal bones (K1/253/1, K1/253/2) have been found, each measuring about 24 mm in length.

3.1.3. Front limb

3.1.3.1. Scapula (Fig. 4(1, 2) and Table 6). The width/length index of the scapula is 64.5. The subscapular fossa is marked by five ridges which provide attachment to tendinous bands of

Table 5
Measurements of the thoracic vertebrae of *M. parvulus* from Kerassia 1
Tableau 5
Dimensions des vertèbres thoraciques de *M. parvulus* de Kerassia 1

	K1/206	K1/268	K1/261	K1/264	K1/216
Length of the centrum	16.6	17.7	18.9	16.8	24.7
Transverse diameter of the centrum, cranially, excluding the rib facets	12.7	13.6	14.3	13.5	22.5
Height of the centrum, cranially	10.1	11.5	12.4	10.7	15.0
Transverse diameter of the centrum, caudally, excluding the rib facets	–	16.1	17.8	15.3	23.0
Height of the centrum, caudally	10.6	12.4	14.6	11.1	14.4
Greatest width at the transverse processes	(42.0)	(34.2)	36.9	38.9	–
Greatest width at the cephalic part of the transverse processes	–	–	–	–	22.8
Greatest width at the caudal part of the transverse processes	–	–	–	–	27.4
Greatest width at the cephalic articular processes or surfaces	25.3	13.7	15.0	14.6	–
Greatest width at the caudal articular processes or surfaces	17.6	14.8	16.7	13.9	12.6

the subscapularis muscle. The teres major fossa is elongated, covering half of the caudal border of the scapula in length, and is well defined medially by an oblique crest. The spine is almost vertically inserted to the body and only slightly overhangs the infraspinous fossa. The acromion projects towards the glenoid cavity but does not pass its level. The glenoid fossa is slightly elongated craniocaudally, with rounded medial and notched lateral edges. The coracoid process, for the coracobrachialis, is almost straight, slender and elongated. It is directed medially and slightly ventrally, and projects to the level of the medial border of the glenoid fossa. The supraglenoid tubercle is not very prominent.

Table 6
Measurements of the scapula of *M. parvulus* from Kerassia 1
Tableau 6
Dimensions de l'omoplate de *M. parvulus* de Kerassia 1

	K1/200, d.	K1/212, s.
Greatest length, parallel to the spine	134.8	–
Greatest width, vertical to the spine	87.0	–
Minimum width at the neck	25.3	26.4
Greatest length of the head	29.5	29.7
Smallest diameter of the head	(19.0)	20.3
Greatest length of the glenoid fossa	24.7	24.8
Length of the coracoid process	–	11.5

3.1.3.2. Humerus (Fig. 4(3) and Table 7). The head of the humerus is almost circular in outline, not mediolaterally compressed, and convex anteroposteriorly. In posterior view, the mediolateral profile is only slightly convex and slopes strongly laterally. A specimen of *Felis attica* from Pikermi (Roussiakis, 2002) has a head that is slightly more compressed mediolaterally, more convex, and without lateral inclination. In medial or

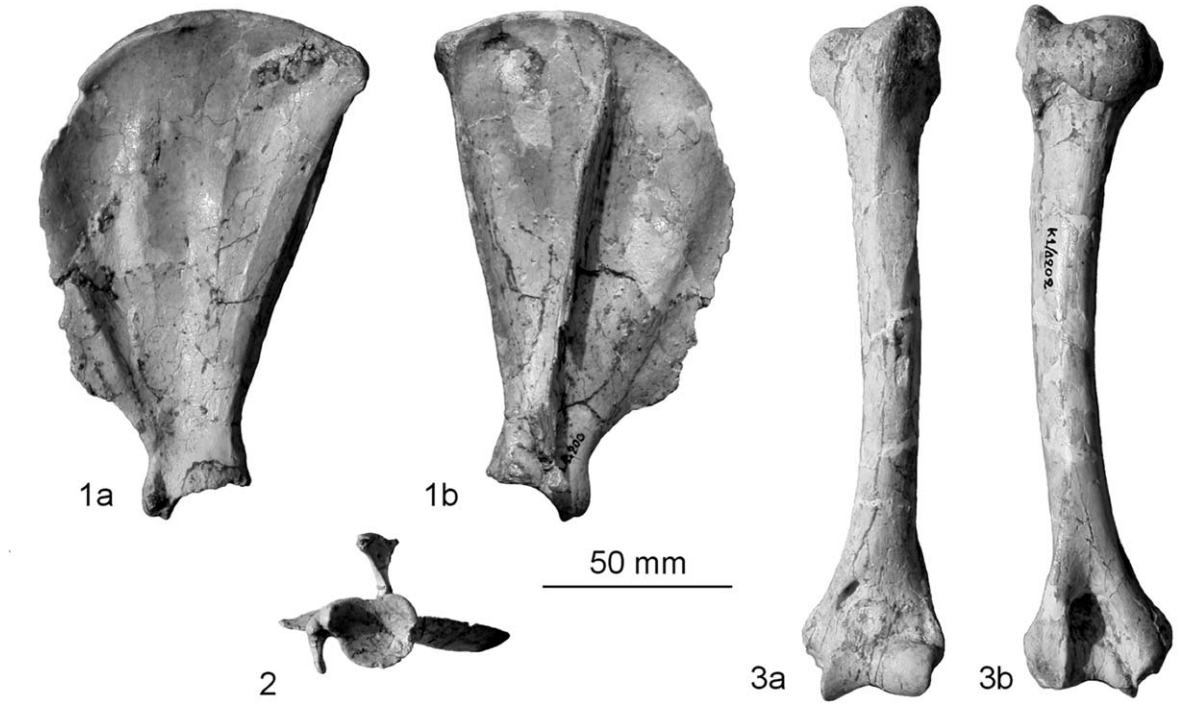

Fig. 4. **1**. Right scapula (K1/200): **a**) medial view **b**) lateral view. **2**. Left scapula (K1/212): proximal view. **3**. Left humerus (K1/202): **a**) anterior view **b**) posterior view. Scale bar 50 mm.
Fig. 4. **1**. Omoplate droite (K1/200): **a**) vue médiale **b**) vue latérale. **2**. Omoplate gauche (K1/212): vue proximale. **3**. Humérus gauche (K1/202): **a**) vue antérieure **b**) vue postérieure. Échelle graphique 50 mm.

Table 7
Measurements of the humerus. (L_{max}: greatest length; DT_{pr}: transverse diameter of the proximal end; DAP_{pr}: anteroposterior diameter of the proximal end; DT_{dia}: transverse diameter at the midshaft; DAP_{dia}: anteroposterior diameter at the midshaft; DT_{dist}: greatest width of the distal end; DAP_{dist}: greatest anteroposterior diameter of the distal end, measured medially; $DT_{distart}$: transverse diameter of the distal articular part, measured vertical to the medial border of the trochlea)
Tableau 7
Dimensions de l'humérus

	L_{max}	DT_{pr}	DAP_{pr}	DT_{dia}	DAP_{dia}	DT_{dist}	DAP_{dist}	$DT_{distart}$
M. parvulus, K1/202, s., Kerassia 1	183.1	37.7	43.5	14.9	19.0	39.4	22.6	28.7
M. parvulus, K4/92/2, s., Kerassia 4	–	36.3	42.6	–	–	–	–	–
M. parvulus, PG98/28, Pikermi	–	–	–	–	–	(39.9)	23.0	27.9
M. parvulus, PG98/29, Pikermi	–	(33.4)	(45.0)	–	–	–	–	–
"*M. anceps*", Hadjidimovo-1 (Kovatchev, 2001)	238	44	62	–	–	56.5	32.5	–
"*P. orientalis*", NHML M 8960, Pikermi	234.3	42.8	59.4	20.5	27.3	59.1	–	39.8

lateral view, the angle formed by the posterior lip of the head that overhangs the neck is very acute, whereas in *F. attica* it is larger and in *Homotherium* from Senèze (Ballesio, 1963: Fig. 25d, f) it is insignificant. The greater tuberosity protrudes slightly beyond the head, while the fossa for the infraspinatus is relatively shallow and level with the head. The tubercle for the attachment of the teres minor is relatively prominent. The lesser tuberosity is obliquely directed in proximal view, and its long diameter is directed from above downwards and posteromedially. In *F. attica* from Pikermi, this tuberosity has the same orientation in proximal view, but in medial view it appears more parallel to the shaft axis. The shaft is anteriorly bowed in lateral view, and mediolaterally compressed. Its mid-section is elliptical, with the long axis directed obliquely (posteromedially–anterolaterally) relative to the distal transverse axis. Its lateral compression is estimated to 77%, comparable with that of the leopard. In the lion it is approximately 70%, and in the cheetah 57% (Hopwood, 1945). The pectoral and deltoid ridges are evident, and converge distally where they blend into the shaft slightly above its mid-length. The coronoid fossa appears deeper and more distinct than the radial fossa. The distal articular surface is mediolaterally elongated, and the surface of the capitulum is smooth without a crest. In anterior view, the medial margin of the trochlea appears oblique to the axis of the shaft, whereas in the cheetah it is almost parallel (Hopwood, 1945). The olecranon fossa has almost equal height and width. A *Machairodus giganteus* humerus from Pikermi (Roussiakis, 2002: Tab. 12) has a relatively greater distal width for its length than *M. parvulus*. The humerus (NHML M8960) from Pikermi, attributed by Pilgrim (1931) to *Paramachairodus orientalis* (Kittl, 1887), and to a lesser degree the humerus of "*M. anceps*" have also relatively wider distal ends (Table 7).

A proximal fragment of a left humerus from the site Kerassia 4 (K4/92/2) is similar in dimensions and morphology to the Kerassia 1 humerus, and can be referred provisionally to *M. parvulus*. The same applies to a distal, and a mediolaterally compressed proximal fragment (AMPG PG98/28 and 29) from Pikermi (Table 7).

3.1.3.3. Ulna (Fig. 5(1) and Table 8). The olecranon process is not posteriorly inclined, and its proximal border is straight and almost perpendicular to the posterior one. The anconeal process is almost level with the coronoid process. In *Homotherium*, the olecranon process is strongly inclined posteriorly, its proximal border slopes backwards, and the anconeal process is not projected so much anteriorly (Ballesio, 1963: Fig. 26; Rawn-Schatzinger, 1992: Fig. 17). The crest at the posteromedial margin of the olecranon process, which gives insertion to the large head of the triceps, is very well developed. It extends distally to the level of the proximal border of the trochlear notch. The lateral olecranon tuberosity (for the anconeus) is thick and located more anteriorly than the medial one (for the medial head of the triceps) which is thinner but higher. According to Kovatchev (2001), in "*M. anceps*" the lateral tuberosity is higher than the medial, but the figures provided are not helpful. In *Homotherium* from Senèze the lateral tuberosity is very high, while the medial one is much reduced (Ballesio, 1963: Fig. 26). Werdelin and Lewis (2001) mention the existence of a groove on the superomedial edge of the trochlear notch in all machairodontines except *Homotherium*, but such a groove could not be observed on the available ulnae of *M. parvulus*. The radial notch faces laterally and its lateral border is rounded. The smooth proximodistal ridge of the trochlear notch, if extended proximally, passes through the lateral tuberosity of the olecranon, as in the leopard. On the contrary, in the lion it passes between the lateral and medial tuberosities of the olecranon, and in the cheetah through the medial tuberosity (Hopwood, 1945). The shaft of the ulna is almost straight in lateral view. In anterior view, its distal part curves laterally on both available specimens. It is mediolaterally compressed, except on its distal third, where it is triangular because of a medial proximodistal crest. The shaft is separated from the distal epiphysis by a constriction visible in lateral view. The distal part of the bone is well developed, and not reduced as in the cheetah (Van Valkenburgh et al., 1990). The distal articular surface for the radius is almost circular in outline, and separated by a deep fossa from the styloid process. The latter is directed strongly posterodistally and is moderately elongated.

3.1.3.4. Radius (Fig. 5(2) and Table 9). In proximal view, the head is elliptical and its long axis is obliquely oriented relative to the transverse axis of the shaft. In anterior view, the head slopes strongly medially. The bicipital tuberosity lies close to the posterolateral margin of the shaft, and its lateral border has a crest, level with the lateral margin of the shaft. The shaft is mediolaterally elongated, and appears bowed anteriorly and medially. The posterior surface of the shaft is flat to slightly convex, and has a proximodistally elongated tubercle, just above its mid-length. Distally and posteriorly, the junction with

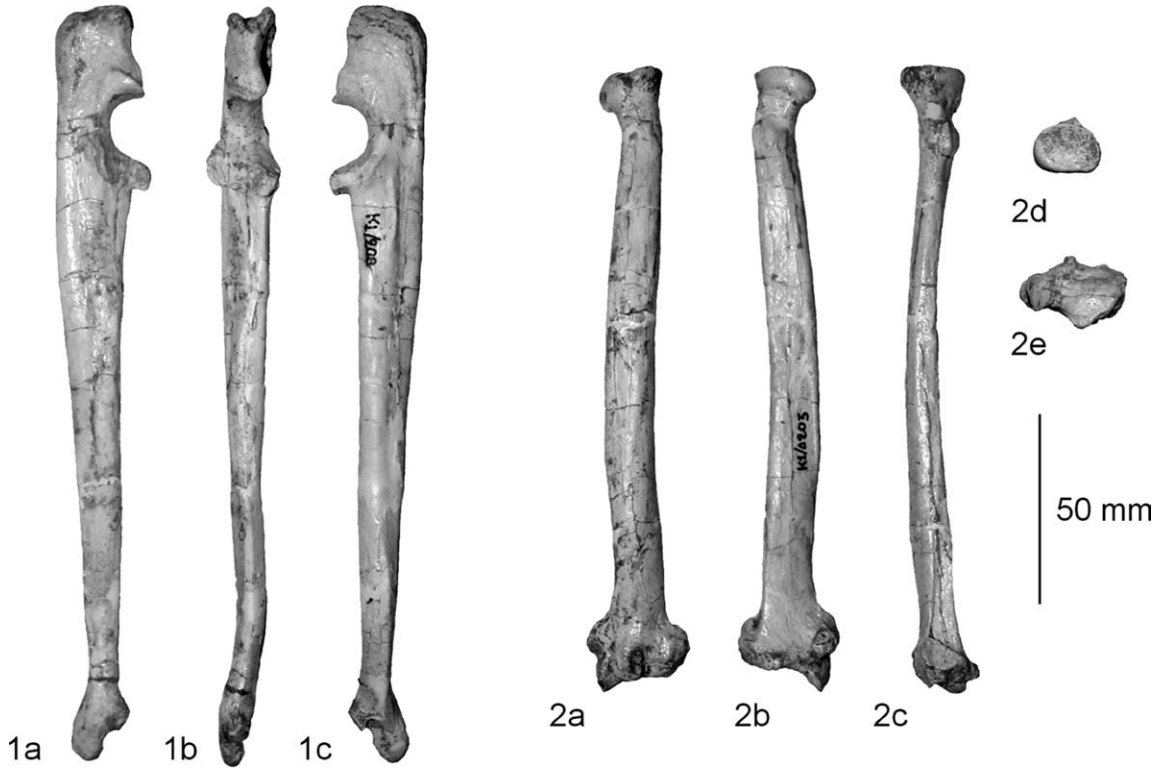

Fig. 5. **1**. Right ulna (K1/208): **a**) lateral view **b**) anterior view **c**) medial view. **2**. Left radius (K1/203): **a**) anterior view **b**) posterior view **c**) lateral view **d**) proximal view **e**) distal view. Scale bar 50 mm.
Fig. 5. **1**. Cubitus droit (K1/208): **a**) vue latérale **b**) vue antérieure **c**) vue médiale. **2**. Radius gauche (K1/203): **a**) vue antérieure **b**) vue postérieure **c**) vue latérale **d**) vue proximale **e**) vue distale. Échelle graphique 50 mm.

Table 8
Measurements of the ulna. (L_{max}: greatest length; $DAPpr_{max}$: anteroposterior diameter measured at the coronoid process; $DAPpr_{min}$: minimum anteroposterior diameter, measured at the greater sigmoid cavity; DAP_{dia}: anteroposterior diameter at the midshaft; DT_{dia}: transverse diameter at the midshaft; DAP_{dist}: greatest anteroposterior diameter of the distal end; DAP_{st}: anteroposterior diameter of the styloid process)
Tableau 8
Dimensions de l'ulna

	L_{max}	DAP_{prmax}	DAP_{prmin}	DAP_{dia}	DT_{dia}	DAP_{dist}	DAP_{st}
M. parvulus, K1/208, d., Kerassia 1	200.8	25.5	14.8	13.4	9.5	16.6	10.3
M. parvulus, K1/204, s., Kerassia 1	200.6	25.7	14.7	13.8	9.3	17.9	(9.6)
"*M. anceps*", Hadjidimovo-1 (Kovatchev, 2001)	248	–	–	–	–	–	–

Table 9
Measurements of the radius. The greatest length (L_{max}) of the "*M. schlosseri*" radius has been estimated from the figure provided by Weithofer (1888: Table 2, Fig. 1). (L_{max}: greatest length; DT_{pr}: transverse diameter of the proximal end; DAP_{pr}: anteroposterior diameter of the proximal end; DT_{neck}: transverse diameter of the neck; DT_{dia}: transverse diameter at midshaft; DAP_{dia}: anteroposterior diameter at midshaft; DT_{dist}: greatest transverse diameter of the distal end; DAP_{dist}: greatest anteroposterior diameter of the distal end)
Tableau 9
Dimensions du radius

	L_{max}	DT_{pr}	DAP_{pr}	DT_{neck}	DT_{dia}	DAP_{dia}	DT_{dist}	DAP_{dist}
M. parvulus, K1/203, s., Kerassia 1	163.5	18.3	13.5	11.3	13.0	8.5	27.1	17.7
M. parvulus, K1/209/1, d., Kerassia 1	164.3	18.6	13.6	11.6	13.4	8.8	26.9	16.6
Felis 3ème esp.", MNHNP PIK 3128, Pikermi	–	–	–	–	–	–	27.4	15.7
"*M. schlosseri*", Pikermi (Weithofer, 1888)	(184)	24	–	–	17	–	37	–
"*P. orientalis*", NHML M 9006A, Pikermi	176.2	24.7	17.1	13.7	15.4	11.0	33.1	20.6
"*Felis* 2ème esp.", MNHNP PIK 3258, Pikermi	200.0	25.5	19.2	17.5	17.6	17.0	38.1	24.5
"*M. anceps*", Hadjidimovo-1 (Kovatchev, 2001)	208	24	21	–	–	–	40	20

the distal epiphysis is rugose and projecting, especially on its lateral part. The lateral surface of the shaft is transversely concave in its distal third. The articular surface for the ulna is elliptical in shape and transversely concave, with its long axis obliquely oriented relative to the long axis of the bone. Moreover, it is clearly offset from the shaft, and its proximal edge is step-like. The anterior surface of the shaft is gently convex. Distally, the groove for the extensor communis digitorum is

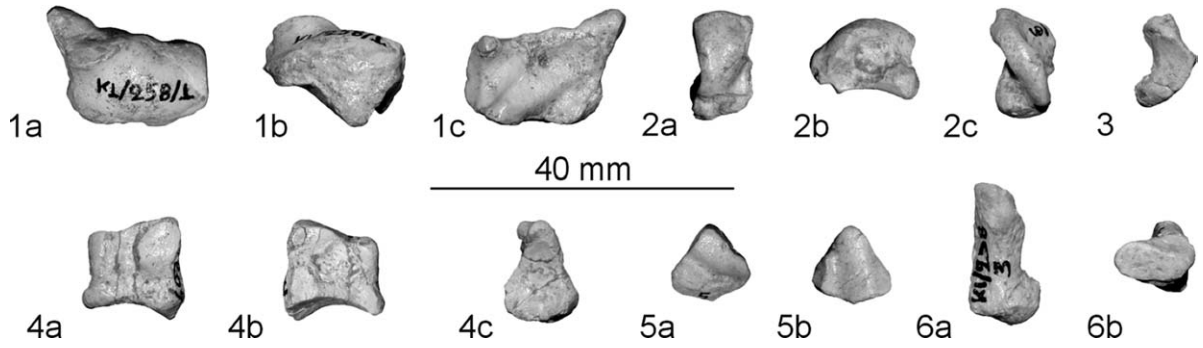

Fig. 6. **1**. Left scapholunar (K1/258/1): **a**) proximal view **b**) anterior view **c**) distal view. **2**. Left magnum (K1/258/6): **a**) distal view **b**) medial view **c**) proximal view. **3**. Left trapezium (K1/258/4): distal view. **4**. Right unciform (K1/209/7): **a**) lateral view **b**) medial view **c**) distal view. **5**. Left trapezoid (K1/258/5): **a**) proximal view **b**) distal view. **6**. Left pisiform (K1/258/3): **a**) upper view **b**) proximal view. Scale bar 40 mm.
Fig. 6. **1**. Scapholunaire gauche (K1/258/1): **a**) vue proximale **b**) vue antérieure **c**) vue distale. **2**. Magnum gauche (K1/258/6): **a**) vue distale **b**) vue médiale **c**) vue proximale. **3**. Trapèze gauche (K1/258/4): vue distale. **4**. Unciforme droit (K1/209/7): **a**) vue latérale **b**) vue médiale **c**) vue distale. **5**. Trapézoïde gauche (K1/258/5): **a**) vue proximale **b**) vue distale. **6**. Pisiforme gauche (K1/258/3): **a**) vue supérieure **b**) vue proximale. Échelle graphique 40 mm.

as wide as, but deeper than the groove for the extensors carpi radialis longior and brevior. The bony projection between these grooves is not very robust. The groove for the extensor ossis metacarpi pollicis is very distinct, whereas the groove for the extensor indicis is scarcely indicated. The styloid process curves slightly posteriorly. Its tip is located slightly medially relative to the medial margin of the shaft in anterior view, as in "*Felis* 3ème espèce" from Pikermi (MNHNP PIK3128) described by Gaudry (1862–1867: Pl. 17, Fig. 8). In "*Felis* 2ème espèce" (MNHNP PIK3258) referred by Gaudry (1862–1867: Pl. 17, Fig. 4) the tip of the styloid process is level with the medial border of the shaft. In the radius of "*M. schlosseri*" from Pikermi figured by Weithofer (1888: Pl. 11, Fig. 1), as well as on the specimen NHML M9006 from Pikermi referred by Pilgrim (1931) to *P. orientalis*, the tip of the styloid process is located more laterally. These specimens have slightly more robust shafts, and wider distal ends for their length compared to *M. parvulus*. A radius of *M. giganteus* from Kerassia 4 (Roussiakis and Theodorou, 2003: Pl. 5, Fig. 3) has a much more robust shaft compared to *M. parvulus*, and the tip of its styloid process is almost level with the medial margin of the shaft.

3.1.3.5. Carpals (Fig. 6 and Tables 10,11). The complete left carpus and one left sesamoid, most probably the radial sesamoid, have been found. From the right carpus, the magnum and the radial sesamoid are missing.

The scapholunar (Fig. 6(1)) has a radius facet that slopes distally on its medial part. The trapezoid facet is divided by a ridge, while in the cheetah it is gently concave (Van Valkenburgh et al., 1990). The posteromedial tubercle is directed medially and distally. A left scapholunar from Pikermi (AMPG PA3686/91) is similar in morphology and dimensions (DT_{max} = 21.3, DAP_{max} = 17.3, H_{max} = 15.1) to the scapholunars of Kerassia, and can also be referred to *M. parvulus*. The articular surface for the radial sesamoid, on the medial side of the posteromedial tubercle, is well indicated in both the Kerassia and Pikermi scapholunars. The trapezium facet is extended posteriorly to the level of the articular surface for the magnum.

The cuneiform articulates proximally with both the ulna and the pisiform. The articular surface for the unciform is concave.

The pisiform (Fig. 6(6)) has a faintly concave facet for the styloid process of the ulna, while the cuneiform facet is flat. The head is elliptical, its large diameter is almost twice as long as its small diameter, and has a groove.

The magnum (Fig. 6(2)) articulates with Mc II through a concave posterior facet and a small flat articular surface on its anteromedial corner. Above the latter there is a small facet for the trapezoid. The magnum also articulates with the trapezoid through a strip-like, narrow articular surface located above and slightly anteriorly to the concave articular surface for Mc II. Distally, the magnum articulates with Mc III and Mc IV through a small triangular surface located posterolaterally. This articular surface is missing in *Homotherium* from Senèze (Bal-

Table 10
M. parvulus, Kerassia 1. Measurements of the scapholunar, cuneiform, trapezium, trapezoid, magnum and unciform. (DT_{max}: greatest transverse diameter; DAP_{max}: greatest anteroposterior diameter; H_{max}: greatest proximo-distal height)
Tableau 10
M. parvulus, Kerassia 1. Dimensions du scapholunaire, du cunéiforme, du trapèze, du trapézoïde, du magnum et de l'unciforme

	DT_{max}	DAP_{max}	H_{max}
Scapholunar, K1/258/1, s., Kerassia 1	21.1	16.9	14.5
Cuneiform, K1/258/2, s., Kerassia 1	8.1	11.5	6.1
Trapezium, K1/258/4, s., Kerassia 1	7.5	12.5	7.5
Trapezoid, K1/258/5, s., Kerassia 1	10.7	10.1	5.7
Magnum, K1/258/6, s., Kerassia 1	9.0	14.0	10.4
Unciform, K1/209/7, d., Kerassia 1	9.9	13.7	13.4

Table 11
Measurements of the pisiform of *M. parvulus* from Kerassia 1. (L_{max}: greatest length; DT_{pr}: greatest diameter of the articular end; H_{pr}: small diameter (height) of the articular end; DT_{head}: transverse diameter of the head; H_{head}: greatest diameter (height) of the head)
Tableau 11
Dimensions du pisiforme de *M. parvulus* de Kerassia 1

	L_{max}	DT_{pr}	H_{pr}	DT_{head}	H_{head}
K1/258/3, s.	18.4	11.1	7.5	7.0	9.9
K1/209/4, d.	18.2	10.9	7.4	7.4	9.8

lesio, 1963). The posterior tubercle is well developed and obliquely oriented.

The trapezium (Fig. 6(3)) articulates with the scapholunar through an almost rectangular and anteroposteriorly concave articular surface. The articular surface for the trapezoid is elongated and larger than that for Mc II.

The trapezoid (Fig. 6(5)) has the shape of an almost equilateral triangle in proximal view. Its proximal articular surface for the scapholunar is flat at its anteromedial corner, but slopes distally. The remaining part of the proximal surface is occupied by a wide groove obliquely oriented from the anterolateral corner to the posteromedial side of the bone. The distal articular surface for Mc II has at its middle a wide and blunt crest that is anteroposteriorly oriented. At the anterolateral corner of the distal surface there is one facet for the magnum. The articular surface for the trapezium occupies almost the entire medial side of the bone.

The unciform (Fig. 6(4)) is wider distally than proximally in anterior view. Its proximal articular surface for the scapholunar is slightly convex anteriorly, and concave posteriorly. On the medial side of the bone and anteriorly, there are two widely connected articular surfaces, for the magnum proximally and for Mc III distally. The proximal one is concave while the distal one is flatter. The unciform also articulates with the magnum through another facet, located posteriorly and distally. On the lateral side, the articular surface for the cuneiform is proximodistally elongated, extended almost to the distal level, convex proximally but concave distally. The distal articular surface is triangular in outline, and concave anteroposteriorly.

3.1.3.6. Metacarpals (Fig. 7 and Table 12). The left metacarpals are fully preserved, as well as some of the right metacarpals. The Mc III is the longest of the metacarpals. When Mcs II to IV are articulated, the proximal end of Mc II projects more proximally, while the others are almost in level. Also in articulation, the head of Mc III lies slightly more distally relative to the head of Mc IV. The heads of Mc II and Mc V lie above the beginning of the heads of Mcs III and IV. The shafts of all metacarpals are straight in anterior view. In lateral view they are straight (Mcs III-V) or slightly bent (Mc II). In all metacarpals, the transverse diameter of the shaft is greater than the anteroposterior diameter.

Mc I is reduced in size, and relatively more robust than in *Homotherium* from Senèze (Ballesio, 1963: Fig. 35) and

Fig. 7. Metacarpals (in proximal and anterior view), and proximal and intermediate phalanges of the left manus (in anterior view). The roman numerals indicate the digits. Ph 1 and 2 dig. II, and Ph 2 dig. IV inversed. Scale bar 50 mm.

Fig. 7. Métacarpiens (en vue proximale et antérieure), et phalanges proximales et intermédiaires du manus gauche (en vue antérieure). Les numéros romains indiquent des doigts. Ph 1 and 2 dig. II, et Ph 2 dig. IV inversées. Échelle graphique 50 mm.

Homotherium serum (Rawn-Schatzinger, 1992: Fig. 24). It resembles in robusticity that of *M. giganteus* from Pikermi (Gaudry, 1862–1867: Pl. 16, Fig. 4). In this species, however, the Mc I is less reduced in length, compared, for example, to Mc III length. The proximal articular surface for the trapezium is almost circular in outline. It occupies more (8.1 mm) than half of the width of the proximal end, and is extended slightly over the anterior surface of the shaft. The tuberosity for the tendon of the extensor ossis metacarpi pollicis is lower in height than

Table 12
Measurements of metacarpals. (L_{max}: greatest length; DT_{pr}: greatest transverse diameter of the proximal end; DAP_{pr}: greatest anteroposterior diameter of the proximal end; DT_{dia}: transverse diameter at the midshaft; DAP_{dia}: anteroposterior diameter at the midshaft; DT_{dist}: transverse diameter of the distal articular end; DAP_{dist}: anteroposterior diameter of the distal articular end)
Tableau 12
Dimensions des métacarpiens

	L_{max}	DT_{pr}	DAP_{pr}	DT_{dia}	DAP_{dia}	DT_{dist}	DAP_{dist}
M. parvulus, Mc I, K1/258/9, s., Kerassia 1	18.1	11.5	7.3	–	–	9.1	8.6
M. parvulus, Mc II, K1/258/10, s., Kerassia 1	55.7	10.6	13.0	7.0	6.5	10.7	10.6
M. parvulus, Mc III, K1/258/11, s., Kerassia 1	65.5	11.8	11.6	7.2	6.4	10.9	10.1
"*M. schlosseri*", Mc III, Pikermi (Weithofer, 1888)	73	–	–	–	–	–	–
M. parvulus, Mc IV, K1/258/12, s., Kerassia 1	62.7	10.0	10.7	6.8	6.3	11.4	(9.6)
M. parvulus, Mc V, K1/258/13, s., Kerassia 1	48.2	9.8	10.7	6.3	5.5	9.7	9.6
"*M. schlosseri*", Mc V, Pikermi (Weithofer, 1888)	55	–	–	–	–	–	–

the trapezium facet. The distal articular surface has a central groove, and is obliquely directed relative to the long axis of the bone.

The proximal articular surface of Mc II is transversely concave. The articular surface for the trapezium is relatively large, and almost circular. The groove for the radial artery on the anterior surface of the shaft is well marked. According to Werdelin and Lewis (2001), this groove is generally present in extant felids, but is not as deep as in machairodonts, and such a deep groove could be a machairodont feature related to robusticity. This groove is absent, however, in *Homotherium* from Senèze (Ballesio, 1963), but present in the Mc II of "*M. schlosseri*" figured by Weithofer (1888: Pl. 9, Fig. 2). On a specimen of *F. attica* from Pikermi (Roussiakis, 2002: Fig. 9.2) there is a circular fossa instead of a groove. Moreover, on this specimen the trapezium facet is more ovoid and elongated proximodistally than in *M. parvulus* from Kerassia.

The proximal articular surface of Mc III is transversely concave. The articular surface for the unciform at the anterolateral corner of the proximal end is well formed.

On Mc IV, the groove that separates the proximal articular surfaces for the unciform and Mc III is faint. On the medial side of the proximal end, a notch separates the anterior and the posterior part of the articular surface for Mc IV.

The proximal articular surface of Mc V for the unciform is strongly convex anteroposteriorly, and extends slightly over the posterior tubercle. Transversely, it is flat, but slopes slightly medially. The lateral tuberosity at the proximal end, for the attachment of the extensor ulnaris muscle, is not particularly projected out of the shaft.

3.1.3.7. Phalanges of the manus (Fig. 7 and Table 13). Various phalanges were found articulated with the metacarpals, but the distal phalanges are poorly preserved.

The proximal phalanx of digit I is the shortest and almost similar in length to Mc I. The other proximal phalanges follow the pattern III, IV, II, V in terms of decreasing length, and are curved in lateral view, especially those of the digits III and IV. The most robust proximal phalanx is that of digit II.

Table 13
Metailurus parvulus, Kerassia 1. Measurements of the proximal phalanges (ph 1) and middle phalanges (ph 2) of the manus. (Abbreviations of measurements as in Table 12)
Tableau 13
Metailurus parvulus, Kerassia 1. Dimensions des phalanges proximales (ph 1) et intermédiaires (ph 2) du manus

	L_{max}	DT_{pr}	DAP_{pr}	DT_{dist}	DAP_{dist}
Ph 1, Mc I, K1/258/14, s.	17.4	10.8	8.1	9.0	6.6
Ph 1, Mc II, K1/258/18, s.	(27.6)	11.4	9.2	–	6.9
Ph 1, Mc III, K1/258/15, s.	31.9	11.5	(8.1)	8.5	7.5
Ph 1, Mc IV, K1/258/21, s.	30.7	11.0	8.5	8.4	6.8
Ph 1, Mc V, K1/259/1, s.	23.5	9.9	8.2	7.2	6.1
Ph 2, Mc II, K1/209/14, d.	21.0	8.9	8.2	8.7	6.9
Ph 2, Mc III, K1/258/16, s.	24.5	9.6	8.8	9.1	7.2
Ph 2, Mc IV, K1/258/22, s.	22.2	(10.3)	(8.4)	7.8	7.1
Ph 2, Mc V, K1/259/2, s.	16.5	8.4	(7.5)	7.1	6.3

The middle phalanges of digits II to V also follow the pattern III, IV, II, V in terms of decreasing length, while the most robust is that of digit V. The middle phalanges are asymmetric, as in extant felids, with the head transversely elongated and projected towards the lateral side. This projection is more pronounced on the middle phalanx of digit III, and insignificant on digit V. The shaft has a triangular cross-section. The distal articular surface of the head is transversely convex, and shows no groove. The orientation of the head varies. It is directed strongly laterally and downwards on the middle phalanx of digit II, and to a lesser degree of digit III, while it is almost perpendicular to the shaft on digit IV, and is directed laterally and slightly upwards on digit V. Such morphological characters and variation are also common in most extant felids. The middle phalanges of the manus of *A. jubatus*, however, are more symmetric, with grooved distal articular surfaces, insignificant angulation of the distal heads, and a shaft with a triangular cross-section only on the middle phalanges of digits II and III (Bryant et al., 1996; Russell and Bryant, 2001).

Of the distal phalanges, only that of digit III is adequately preserved. The greatest length of its proximal part measures 20.8 mm, and its transverse diameter measures 7.5 mm.

3.1.4. Hind limb

3.1.4.1. Femur (Fig. 8(1) and Table 14). The tip of the greater trochanter lies only slightly higher than the proximal end of the head. The head is rounded, and in medial view the fovea capitis seems to open slightly posteriorly. In posterior view, the proximal end of the intertrochanteric crest curves medially, and the intertrochanteric fossa does not extend to the level of the lesser trochanter. The distal part of the greater trochanter flares laterally, and forms a crest that is probably for the gluteus maximus. The lesser trochanter lies medially relative to the long axis of the shaft. The mid-shaft shape index ($DT_{dia} \times 100/DAP_{dia}$) is very large (126.3), but the shaft is probably anteroposteriorly compressed and a slightly lower value could be expected. The shaft certainly has an ovoid mid-section, however, with a transverse diameter that is greater than the anteroposterior one. According to Lewis (1997) this is associated with reduced cursoriality but increased load-bearing abilities. Moreover, the shaft is bowed anteriorly, a feature more typical of felids with jumping abilities (Rawn-Schatzinger, 1992). The lateral border of the shaft is very acute distal to the greater trochanter, forming a crest that extends almost to the mid-length of the shaft. This crest, as well as the lateral flaring of the greater trochanter, probably increases the attachment area of the abductors of the thigh. The patellar groove is shallow, and its edges converge proximally. In posterior view, the distal articular condyles are widely separated, and the intercondyloid fossa is not parallel-sided, but appears wider proximally. The pits for the popliteus muscle and the external lateral ligament of the knee-joint, on the lateral surface of the distal epiphysis, are well marked, whereas the pit for the extensor longus digitorum is faint. The pit for the internal lateral ligament of the knee joint, on the medial surface of the distal epiphysis, is also well marked.

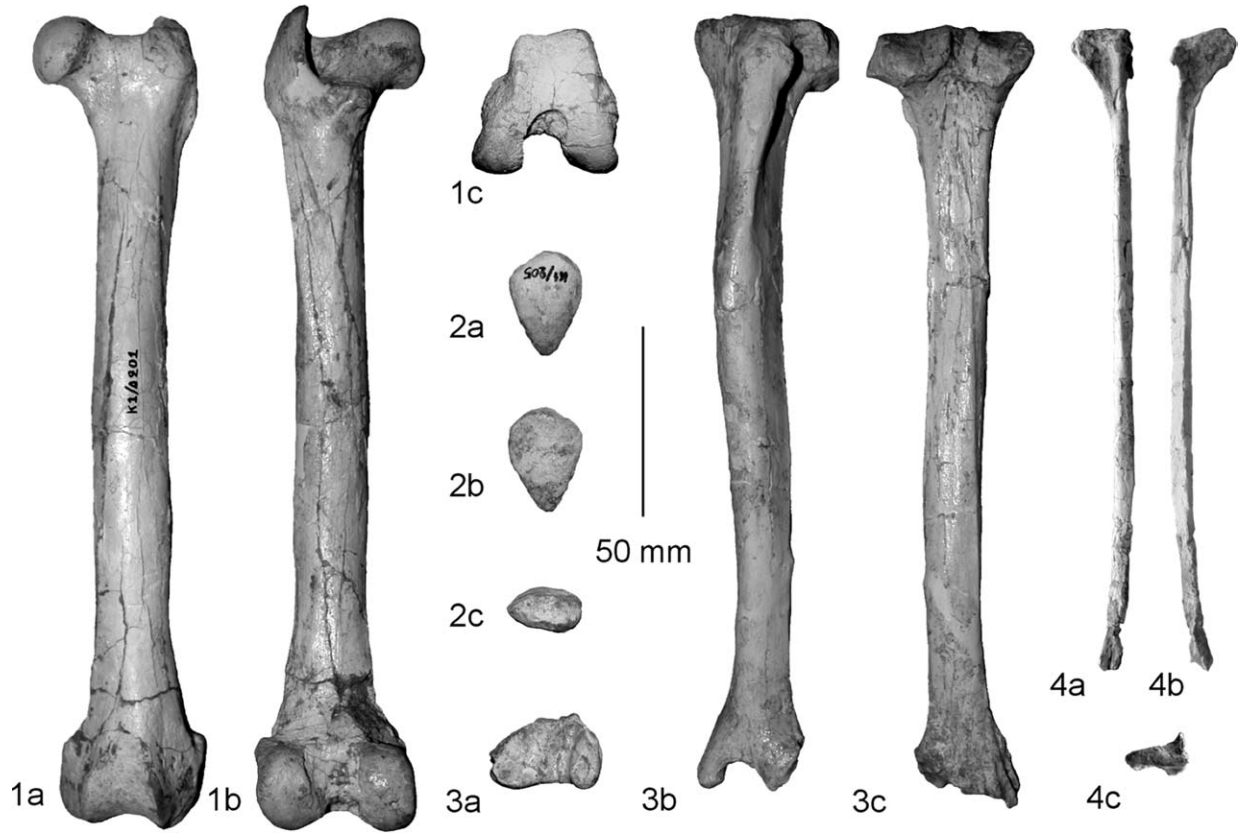

Fig. 8. **1**. Left femur (K1/201): **a**) anterior view **b**) posterior view **c**) distal view. **2**. Right patella (K1/205): **a**) anterior view **b**) posterior view **c**) upper view. **3**. Left tibia (K1/252/26): **a**) distal view **b**) anterior view **c**) posterior view. **4**. Left fibula (K1/252/27): **a**) lateral view **b**) medial view **c**) proximal view. Scale bar 50 mm.
Fig. 8. **1**. Fémur gauche (K1/201): **a**) vue antérieure **b**) vue postérieure **c**) vue distale. **2**. Rotule droite (K1/205): **a**) vue antérieure **b**) vue postérieure **c**) vue supérieure. **3**. Tibia gauche (K1/252/26): **a**) vue distale **b**) vue antérieure **c**) vue postérieure. **4**. Péroné gauche (K1/252/27): **a**) vue latérale **b**) vue médiale **c**) vue proximale. Échelle graphique 50 mm.

Table 14
Measurements of the femur. (L_{max}: greatest length; DT_{pr}: greatest transverse diameter of the proximal end; DT_{cap}: transverse diameter of the caput femoris; DAP_{cap}: anteroposterior diameter of the caput femoris; DT_{dia}: transverse diameter at the midshaft; DAP_{dia}: anteroposterior diameter at the midshaft; DT_{dist}: greatest transverse diameter of the distal end; DAP_{dist}: greatest anteroposterior diameter of the distal end)
Tableau 14
Dimensions du fémur

	L_{max}	DT_{pr}	DT_{cap}	DAP_{cap}	DT_{dia}	DAP_{dia}	DT_{dist}	DAP_{dist}
M. parvulus, K1/201, s., Kerassia 1	216.0	44.1	19.9	20.7	19.7	(15.6)	40.4	40.7
"*M. anceps*", Hadjidimovo (Kovatchev, 2001)	285	–	24.5	–	–	–	–	–

Compared to a femur of *M. giganteus* from Pikermi (Roussiakis, 2002: Fig. 12.2), the *M. parvulus* femur has a slightly wider distal end for its length, and probably a more robust shaft. The tibial condyles are relatively more widely separated, and the greater trochanter more laterally flared. A *F. attica* femur from Pikermi (NHML M9011) has a much more slender distal epiphysis for its length compared to *M. parvulus*.

3.1.4.2. Patella (Fig. 8(2)). The height of the patella measures 27.8 mm, its transverse diameter 19.7 mm, and its anteroposterior diameter (thickness) 10.0 mm. The articular surface for the femur is almost circular, and occupies the whole posterior surface of the bone, except close to the apex. This facet is a little concave from above downwards and convex transversely. The apex is pointed. Compared to the patella of "*M. anceps*"

Table 15
Measurements of the tibia. (Abbreviations of measurements as in Table 14)
Tableau 15
Dimensions du tibia

	L_{max}	DT_{pr}	DAP_{pr}	DT_{dia}	DAP_{dia}	DT_{dist}	DAP_{dist}
M. parvulus, K1/252, s., Kerassia 1	207.8	42.2	42.0	15.2	19.4	28.3	19.2
"*Felis* 2ème esp.", MNHNP PIK 3256, Pikermi	225.0	40.0	42.1	15.0	19.2	29.3	17.8
"*Felis* 1ème esp.", MNHNP PIK 3255, Pikermi	–	–	–	–	–	36.6	23.9
"*M. anceps*", Hadjidimovo-1 (Kovatchev, 2001)	265	53	40	–	–	36	24

(Kovatchev, 2001: Pl. 4, Fig. 4), that of *M. parvulus* is not so narrow transversely.

3.1.4.3. Tibia (Fig. 8(3) and Table 15). The tibia of *M. parvulus* is elongated relative to the femur. The tibial crest is slightly convex anteriorly in lateral view, whereas in the cheetah it is concave (Van Valkenburgh et al., 1990). The shaft appears slightly sigmoid in anterior view and its mid-section is subtriangular. On the posterior surface, the intercondyloid fossa is shallow and two distinct oblique crests define areas of muscle attachment. The insertion area of the popliteus muscle, which rotates the thigh medially, occupies a very small area confined to the most proximal and medial part of the shaft. The area of origin of the flexor longus hallicus muscle, which flexes the phalanges, is greatly expanded, and occupies most of the posterior surface of the shaft. On the other hand, the surface for the tibialis posterior, which extends the foot, is reduced and confined to a narrow strip between the other two areas, almost to the proximal fourth of the posterior surface of the shaft. Distally, the groove for the tendon of the tibialis posterior is especially marked, and deeper but narrower than that for the tendon of the flexor longus digitorum. The medial malleolus is not projected distally, though slightly more so than the lateral part of the distal epiphysis, and is directed medially. The distal articular surface for the fibula is poorly preserved. Compared to a *M. giganteus* tibia from Pikermi (Roussiakis, 2002: Fig. 12.3), in *M. parvulus* the surface for the flexor longus hallicus is larger, while that for the tibialis posterior is smaller. Moreover, the *M. parvulus* tibia has a relatively less robust shaft for its length. The distal tibial fragment from Pikermi (MNHNP PIK3255) described by Gaudry (1862–1867: Pl. 17, Fig. 2) as "*Felis* 1ère espèce" is larger in its dimensions (Table 15). Its medial malleolus is almost level with the lateral part of the distal epiphysis, as in *M. parvulus* from Kerassia 1, but more vertical. The complete tibia (MNHNP PIK3256) figured by Gaudry (1862–1867: Pl. 17, Fig. 7) as "*Felis* 2ème espèce" is slightly greater in length (Table 15), and slightly less robust. Its shaft is straighter, and its medial malleolus is more vertical and more distally projected. Compared to *M. parvulus*, a *F. attica* tibia from Pikermi (NHML M9010) has a slightly less robust shaft for its length, and its medial malleolus extends more distally.

3.1.4.4. Fibula (Fig. 8(4)). The shaft of the fibula is much curved, and has a marked proximodistal medial keel. A distal portion of its diaphysis is missing, and its greatest length (approx. 186.0 mm) has been calculated after the articulation of the preserved proximal and distal parts to the tibia. The prox-

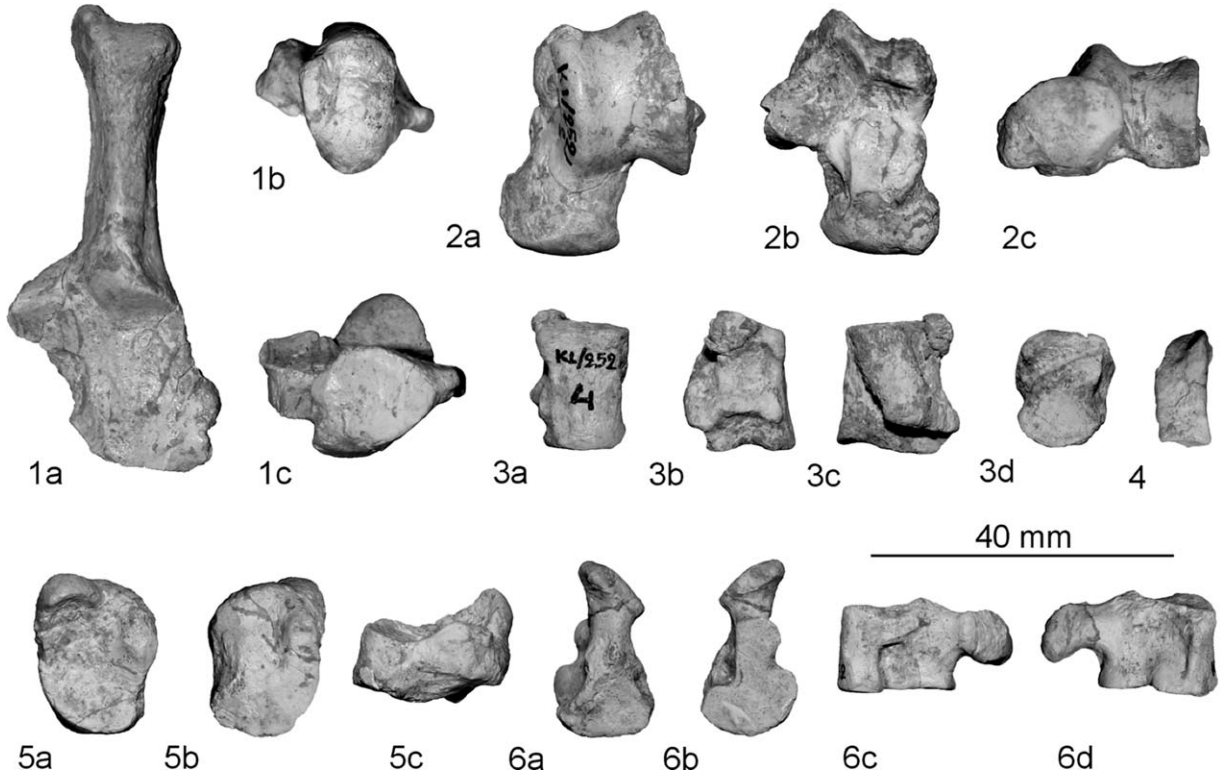

Fig. 9. **1**. Left calcaneum (K1/252/1): **a**) anterior view **b**) proximal view **c**) distal view. **2**. Left astragalus (K1/252/2): **a**) anterior view **b**) posterior view **c**) distal view. **3**. Left cuboid (K1/252/4): **a**) anterior view **b**) medial view **c**) posterior view **d**) distal view. **4**. Left entocuneiform (K1/252/6): lateral view. **5**. Left navicular (K1/252/3): **a**) proximal view **b**) distal view **c**) lateral view. **6**. Left ectocuneiform (K1/252/7): **a**) proximal view **b**) distal view **c**) lateral view **d**) medial view. Scale bar 40 mm.

Fig. 9. **1**. Calcanéum gauche (K1/252/1): **a**) vue antérieure **b**) vue proximale **c**) vue distale. **2**. Astragale gauche (K1/252/2): **a**) vue antérieure **b**) vue postérieure **c**) vue distale. **3**. Cuboïde gauche (K1/252/4): **a**) vue antérieure **b**) vue médiale **c**) vue postérieure **d**) vue distale. **4**. Entocunéiforme gauche (K1/252/6): vue latérale. **5**. Naviculaire gauche (K1/252/3): **a**) vue proximale **b**) vue distale **c**) vue latérale. **6**. Ectocunéiforme gauche (K1/252/7): **a**) vue proximale **b**) vue distale **c**) vue latérale **d**) vue médiale. Échelle graphique 40 mm.

Table 16
Measurements of the astragalus. (H_{max}: greatest proximodistal height; $H_{trochlat}$: height of the lateral trochlea; DT_{head}: greatest transverse diameter of the head; DAP_{head}: anteroposterior diameter of the head; DT_{max}: greatest transverse diameter)
Tableau 16
Dimensions de l'astragale

	H_{max}	$H_{trochlat}$	DT_{head}	DAP_{head}	DT_{max}
M. parvulus, K1/252/2, s., Kerassia 1	34.7	22.4	18.3	12.5	27.9
M. parvulus, K1/105, d., Kerassia 1	33.1+	–	18.4	12.2	27.3
"*Felis* 1ère esp.", MNHNP PIK 3041, Pikermi	41.3	26.4	19.6	16.0	34.0
"*M. anceps*", Hadjidimovo-1 (Kovatchev, 2001)	42	–	23	12	–

Table 17
Measurements of the calcaneum. (H_{max}: greatest proximodistal height; DT_{tub}: greatest transverse diameter of the tuber calcanei; DAP_{tub}: greatest anteroposterior diameter of the tuber calcanei; DT_{col}: transverse diameter at the mid-height of the neck; DAP_{col}: anteroposterior diameter at the mid-height of the neck; DT_{max}: greatest transverse diameter; DAP_{max}: greatest anteroposterior diameter; DT_{dist}: greatest transverse diameter of the distal articular end; DAP_{dist}: anteroposterior diameter of the distal articular end)
Tableau 17
Dimensions du calcanéum

	H_{max}	DT_{tub}	DAP_{tub}	DT_{col}	DAP_{col}	DT_{max}	DAP_{max}	DT_{dist}	DAP_{dist}
M. parvulus, K1/252/1, s., Kerassia 1	61.9	14.3	19.7	9.3	18.3	28.5	23.3	17.9	13.5
"*Felis* 1ère esp.", MNHNP PIK 3041, Pikermi	74.6	19.0	21.6	12.3	23.8	35.4	28.2	(19.0)	16.0
MNHNP PIK 3286, Pikermi	74.8	19.6	21.6	12.0	23.2	34.3	28.2	19.3	16.2
."*M. anceps*.", Hadjidimovo-1 (Kovatchev, 2001)	76.5	–	–	–	–	–	–	–	–

Table 18
Measurements of the navicular and the cuboid. (Abbreviations of measurements as in Table 10)
Tableau 18
Dimensions du naviculaire et du cuboïde

	H_{max}	DT_{max}	DAP_{max}
Navicular, *M. parvulus* K1/252/3, s., Kerassia 1	15.6	16.0	21.6
Navicular, "*M. anceps*" Hadjidimovo-1 (Kovatchev, 2001)	–	–	25
Cuboid, *M. parvulus* K1/252/4, s., Kerassia 1	18.9	14.1	14.7
Cuboid, "*Felis* 1ère esp." MNHNP PIK 3041, Pikermi	23.9	17.5	19.6

Table 19
Measurements of the cuneiforms. (Abbreviations of measurements as in Table 10)
Tableau 19
Dimensions des cunéiformes

	H_{max}	DT_{max}	DAP_{max}
M. parvulus, 1st, K1/252/6, s., Kerassia 1	15.8	6.9	8.0
M. parvulus, 2nd, K1/252/5, s., Kerassia 1	8.8	6.5	9.8
M. parvulus, 2nd, K1/251/3, d., Kerassia 1	8.5	6.5	9.6
M. parvulus, 3rd, K1/252/7, s., Kerassia 1	13.2	13.3	23.5
"*Felis* 1ère esp.", 3rd, MNHNP PIK 3041, Pikermi	(17.0)	14.2	–

imal articular surface for the tibia is anteroposteriorly elongated (14.2 × 6.1 mm). The posterior tubercle is well developed, projected clearly from the shaft, and directed anteriorly. On the medial surface of the proximal epiphysis and posteriorly there is a prominent crest, probably for the flexor longus digitorum muscle. The distal epiphysis is not well preserved.

3.1.4.5. Tarsals (Fig. 9 and Tables 16–19). The calcaneum (Fig. 9(1)) has an anteroposteriorly elongated tuber and its anterior border is angular in proximal view. Conversely, the tuber is almost circular in *F. attica* from Pikermi (Roussiakis, 2002) and "*Felis* 1ère espèce" from Pikermi (Table 17, MNHNP PIK 3041; Gaudry, 1862–1867, Pl. 17, Fig. 3). The medial border of the tuber is clearly higher than the lateral one, but the groove for the tendo achillis is not deep. The distal articular surface for the cuboid is slightly concave anteroposteriorly, slopes strongly distolaterally, and is especially ovoid in outline, with large axis anterolaterally-posteromedially oriented. This articular surface is almost circular in *F. attica* (Roussiakis, 2002). At the medial border of the cuboid facet there is a small articular surface for the navicular. This facet is also present in *Homotherium* from Senèze and in *Smilodon* (Ballesio, 1963). In *F. attica* from Pikermi the navicular contacts the calcaneum, but no clear articular surface is visible on the latter. Just anteriorly to the articular surface for the navicular, there is a small facet for the head of the astragalus, connected by a narrow ridge to the sustentacular facet. Such a narrow connection, although slightly less evident, is also present in *F. attica*. It is interesting that, according to Werdelin and Lewis (2001), in *Panthera* there is no such connection in the calcaneum, not even in species with a connection in the corresponding facets of the astragalus.

The astragalus (Fig. 9(2)) has an elongated head, the neck is not shortened, and the medial ridge of the trochlea is not prolonged onto the neck. The articular surface for the calcaneum, behind the neck, is almost circular in outline and connected through a narrow ridge to the calcaneal articular surface of the head. According to Werdelin and Lewis (2001) some species of *Panthera*, such as the lion, the leopard and the jaguar, have such a narrow connection, while others, such as the tiger, do not. A narrow connection is also present in the astragalus referred to as "*Machairodus*" *orientalis* by Kittl (1887: Pl. 14, Fig. 5), and possibly in *F. attica* (Beaumont, 1986: Fig. 4b). In *Homotherium* from Senèze, this connection is much wider (Ballesio, 1963: Fig. 49), while *Homotherium* from Incarcal varies significantly in this character (Galobart et al., 2003: Pl. 12, Fig. C1–4).

The navicular (Fig. 9(5)) is anteroposteriorly elongated. Its posteromedial and posterolateral tubercles are not separated by a groove. The proximal articular surface is concave and ellipsoid in shape. On the lateral side there is a large ovoid facet located at the posterior half and proximally, and a smaller, circular one located anteriorly and distally. These surfaces, both of which serve for the articulation with the cuboid, are connected to each other. Above the posterolateral facet there is a smaller one for the calcaneum. A *F. attica* specimen from Pikermi (Roussiakis, 2002) also has an ellipsoid proximal articular surface but the posterior tubercles are separated by a groove, while there is no clear articular surface for the calcaneum. An articular surface for the calcaneum exists in *Homotherium* from Senèze and *Smilodon*, but the former lacks the articular surface for the cuboid (Ballesio, 1963).

The entocuneiform (Fig. 9(4)) is proximodistally elongated. The proximal articular surface for the navicular is concave and slopes anterolaterally. The distal articular surface for the rudimentary Mt I is anteroposteriorly elongated. At the lateral side and almost at mid-height there is a circular and concave articular surface, probably for the mesocuneiform.

The mesocuneiform has slightly anteroposteriorly elongated proximal and distal articular surfaces. The proximal one is ovoid in shape, slightly concave transversely, and slopes slightly laterally. The distal articular surface has a notch at its posterolateral border, and appears slightly convex transversely.

The ectocuneiform (Fig. 9(6)) articulates proximally with the navicular through a triangular articular surface. In *F. attica*, this articular surface is almost circular. At the proximal part of the lateral side there is a large, anteroposteriorly elongated articular surface for the cuboid. The same articular surface in *F. attica* is relatively larger, and almost circular. At the distal part of the lateral side, the ectocuneiform articulates with Mt IV through two small articular surfaces located anteriorly and posteriorly. In posterior view, the posterior tubercle is ovoid and is directed from above downwards and medially. In *F. attica* this tubercle is also ovoid, but almost vertical.

The cuboid (Fig. 9(3)) has the form of a trapezium in anterior view, with its height greater than its width, and its width greater proximally than distally. The proximal articular surface is transversely elongated and presents a posterior notch. The articular surfaces for the navicular are connected, and occupy the whole proximal part of the medial side. A *F. attica* cuboid from Pikermi (Roussiakis, 2002) is relatively shorter for its width, and there is no clear connection between the navicular facets. In *Homotherium* from Senèze there is no articulation with the navicular (Ballesio, 1963). The articular surface for

Fig. 10. Metatarsals (in proximal and anterior view), and proximal and intermediate phalanges of the left pes (in anterior view). The roman numerals indicate the digits. Ph 1 dig. III, inversed. Scale bar 50 mm.
Fig. 10. Métatarsiens (en vue proximale et antérieure), et phalanges proximales et intermédiaires du pes gauche (en vue antérieure). Les numéros romains indiquent des doigts. Ph 1 dig. III, inversée. Échelle graphique 50 mm.

Table 20
Measurements of the metatarsals. (Abbreviations of measurements as in Table 12)
Tableau 20
Dimensions des métatarsiens

	L_{max}	DT_{pr}	DAP_{pr}	DT_{dia}	DAP_{dia}	DT_{dist}	DAP_{dist}
M. parvulus, Mt I, K1/251/4, d., Kerassia	11.6	7.1	7.8	–	–	–	–
"*M. anceps*", Mt I, d., Hadjidimovo-1 (Kovatchev, 2001)	18	–	–	–	–	–	–
M. parvulus, Mt II, K1/252/18, s., Kerassia 1	77.2	9.6	13.9	7.7	6.5	10.9	11.1
"*M. anceps*", Mt II, Hadjidimovo-1 (Kovatchev, 2001)	91	–	–	–	–	–	–
"*Felis* 1ère esp.", Mt II, MNHNP PIK 3041, s., Pikermi	(93.1)	(11.5)	17.9	(9.5)	8.2	14.0	13.5
M. parvulus, Mt III, K1/252/8, s., Kerassia 1	86.1	13.9	17.6	10.1	7.9	12.1	12.0
"*Felis* 1ère esp.", Mt III, MNHNP PIK 3041, Pikermi	(102.0)	(15.6)	21.2	(12.6)	10.2	13.2	14.4
"*M. anceps*", Mt III, d., Hadjidimovo-1 (Kovatchev, 2001)	101	–	–	–	–	–	–
M. parvulus, Mt IV, K1/252/12, s., Kerassia 1	89.0	9.9	15.1	8.6	8.5	11.3	11.4
"*M. anceps*", Mt IV, d., Hadjidimovo-1 (Kovatchev, 2001)	101	–	–	–	–	–	–
M. parvulus, Mt V, K1/252/22, s., Kerassia 1	77.4	9.8	14.1	6.2	5.6	10.1	(10.0)
"*M. anceps*", Mt V, d., Hadjidimovo-1 (Kovatchev, 2001)	86	–	–	–	–	–	–

the ectocuneiform is anteroposteriorly elongated, whereas it is more ovoid and relatively larger in *F. attica*. The distal articular surface for Mts IV and V is anteroposteriorly concave, subtriangular in shape, has a notch on its medial border, and an anteroposterior diameter that is greater than its mediolateral one.

3.1.4.6. Metatarsals (Fig. 10 and Table 20). The Mt IV is the longest of the metatarsals. When Mts II to V are articulated, the heads of Mt III and Mt IV are almost level, while the heads of Mt II and Mt V are level with each other, but above those of Mt III and Mt IV. The shafts of Mt III to V are slightly bowed anteriorly, whereas the shaft of Mt II is almost straight. In anterior view, Mt II and Mt IV are almost straight, while Mt V curves laterally. Mt III is the most robust metatarsal and the section at its mid-length is oval and transversely elongated. The cross section of Mt II and Mt IV is less elongated transversely, whereas that of Mt V is almost circular.

Mt I is rudimentary and lacks a distal phalanx facet, as in most felids except *Proailurus* and *Pseudaelurus validus* (Rothwell, 2003).

Mt II has a subtriangular proximal articular surface with a relatively prominent lateral notch. Medially it articulates with the entocuneiform, while there is no distinct facet for Mt I. The anterolateral facet for Mt III and the ectocuneiform is clearly taller than the posterolateral facet and its proximal border almost coincides with the anterolateral border of the proximal articular surface. An *F. attica* specimen from Pikermi (Roussiakis, 2002) is generally similar, but its anterolateral facet for the ectocuneiform is slightly more widely separated from the proximal articular surface.

Mt III has a posterior tubercle that is circular in posterior view and with its proximalmost part at a slightly higher level than the proximal articular surface, as is also the case in *F. attica* from Pikermi (Roussiakis, 2002). The posterolateral surface for Mt IV is flat and circular, faces anterolaterally, and extends to the proximal articular level. The same articular surface in an *M. giganteus* specimen from Pikermi (Roussiakis, 2002) is at the same level, but slightly elongated proximodistally and with sigmoid proximodistal profile. In *F. attica* from Pikermi this facet is circular and concave. The anterior articular surface for Mt IV is concave and lies below the proximal articular level, as in *F. attica* and *M. giganteus* from Pikermi.

Mt IV has posterior tubercle directed posteromedially-anterolaterally in proximal view. In posterior view, this tubercle is transversely elongated and almost horizontal, as also in specimens of *M. giganteus* and *F. attica* from Pikermi.

The proximal end of Mt V has two tubercles: a high anterolateral one for the peroneus brevis, and a shorter posterior one for the peroneus longus. The anterolateral tubercle is more robust than the posterior one.

3.1.4.7. Phalanges of the pes (Fig. 10 and Table 21). The available phalanges of the pes are fewer in number than those of the manus but they were also found in articulation with their respective metatarsals. Their general morphology is not different from that of the corresponding phalanges of the manus.

The proximal phalanges of the pes follow the III, IV, II, V pattern in terms of decreasing length, as do the proximal phalanges of the manus. The proximal phalanges of Mt II to IV are only slightly greater in length than the respective phalanges of the manus. Conversely, the proximal phalanx of Mt V is much longer than the proximal phalanx of Mc V, but has an equally wide shaft. Proximal phalanx III has the widest shaft, but is only slightly more robust than proximal phalanx IV. Proximal phalanx V has the slenderest shaft, and is least robust.

Middle phalanx III is missing. Of the remaining middle phalanges of the pes, that of digit IV is the longest and least robust, and that of digit V is the shortest. The lateral projection of the head of the middle phalanges of the pes is pronounced on digits II and IV, but insignificant on digit V. In all cases, this projection is smaller than on the corresponding phalanges of the manus. The head slopes slightly downwards and laterally on the middle phalanx of digit II, while on the remaining available middle phalanges of the pes it is almost perpendicular to the shaft axis. The distal articular surfaces of the middle phalanges have a slight anteroposterior groove, absent in the middle phalanges of the manus.

Of the distal phalanges of the pes, only that of digit II is completely preserved. It has a blade-like, deep but short claw core, very narrow transversely, with a slightly curved dorsal margin. The greatest length of its proximal part is 16.4 mm, and its width 7.0 mm.

Available data (Roussiakis, 2002) indicate that the proximal phalanges of the pes in *F. attica* from Pikermi are probably shorter relative to the metatarsals than in *M. parvulus*. The $LPh1 \times 100/L_{max}$Mt IV index for example is 30.1 in *F. attica* and 35.8 in *M. parvulus*.

4. Body mass prediction and limb proportions

The present material of *M. parvulus* corresponds to an animal about 50 cm in height at the shoulders. This height is com-

Table 21
M. parvulus, Kerassia 1. Measurements of the proximal phalanges (ph 1) and middle phalanges (ph 2) of the pes. (Abbreviations of measurements as in Table 12)
Tableau 21
M. parvulus, Kerassia 1. Dimensions des phalanges proximales (ph 1) et intermédiaires (ph 2) du pes

	L_{max}	DT_{pr}	DAP_{pr}	DT_{dist}	DAP_{dist}
Ph 1, Mt II, K1/251/2, d.	28.4	11.5	9.9	9.7	6.9
Ph 1, Mt III, K1/217, d.	33.7	12.9	9.7	9.9	7.9
Ph 1, Mt IV, K1/252/13, s.	31.9	(11.8)	9.2+	9.8	(6.9)
Ph 1, Mt V, K1/52/23, s.	27.2	9.6	8.7	7.9	6.0
Ph 2, Mt II, K1/252/20, s.	18.1+	9.9	7.5+	8.8	6.3
Ph 2, Mt IV, K1/252/16, s.	22.6	9.8	9.0	8.5	6.7
Ph 2, Mt V, K1/252/24, s.	17.3	8.5	7.6	7.5	5.9

parable to that of a small-sized leopard or a clouded leopard. However, it is not known whether this size corresponds to the average size of the species, since many extant felid species vary significantly in size. Unfortunately, it was not possible to find adequate metric data for the robusticity of extant felids. Based on the average lengths and circumferences of the stylopodium and some of the zygopodium elements of extant felids provided by Christiansen (1999), *M. parvulus* appears more robustly built for these limb-bone elements than the cheetah, the lynx, the caracal, or the serval, but less than the leopard. In general, *M. parvulus* appears similar to the snow leopard in robusticity.

The available dental and postcranial material of *M. parvulus* enable us to estimate its body mass. Van Valkenburgh (1990) used the length of M_1 as predictor of body weight. Applying the regression for the felids provided by her, the body mass for *M. parvulus* is estimated to have been 42 kg. The postcranial elements are generally considered better body mass predictors than the craniodental predictors (Andersson, 2004). Anyonge (1993) used various parameters as body weight predictors. Five of these parameters are employed here: the humeral and femoral length (HL and FL), the humeral and femoral circumference (HC and FC), and the distal articular area of the femur (FDA). Applying the felid regressions provided by Anyonge (1993), the body mass estimates of *M. parvulus* range between 33 kg (HL) and 48.6 kg (FC), while the derived values from FDA, FL, and HC were 34, 36, and 37.5 kg, respectively. The mean value obtained from all parameters used has been found to be 37 kg. Excluding the lengths, which are not good body mass predictors (Anyonge, 1993), the mean value obtained is 40 kg. Limb-bone dimensions as body mass predictors are also used by Egi (2001). Ten of the predictors and the scansorial regressions used by her are applied here. According to Egi (2001) the shaft cross-sectional properties of the humerus, the femur and in lesser degree the tibia are better body mass predictors. The estimated body mass of *M. parvulus* using the total subperiosteal area of the humerus, the femur and the tibia has been found to be 41.5, 50, and 45 kg, respectively. Based on the lengths of the above three elements, the body weight of *M. parvulus* has been found 34–40 kg, but lengths are not considered good body mass estimators (Egi, 2001). The values derived from the volume and surface area of the femoral head are 33 and 34 kg, respectively. By contrast, the articular volume and surface of the humeral head indicate a value of 46–47 kg. Length parameters excluded, the mean value of the estimates derived from the humerus was found to be about 45 kg, as also that derived from the tibia, while the mean value of the estimates derived from the femur has been found 39 kg. The mean value of all estimates (length parameters inclusive) was found 41 kg, slightly lower than that (43 kg) obtained from all estimates excluding predictions based on lengths. The detransformation bias (Smith, 1993) included in the above estimations has not been corrected, and a slight difference between the predicted body mass value and actual body mass value is expected. However, all three methods applied here resulted in body mass values higher than that reported by Legendre and Roth (1988). These authors used the crown area ($L \times W$) of M_1 as a predictor of the body mass and estimated a body weight of 22 kg for *Metailurus minor* Zdansky, 1924, a species considered synonym of *M. parvulus*.

Table 22
Relative limb proportions. (Data for extant species are according to Gonyea (1976a), methodology according to Hildebrand (1952). All indices of *M. parvulus* have been estimated for the left limb-bone elements)
Tableau 22
Rapports des longueurs des segments des membres

	Humeroradial index	Femorotibial index	Intermembral index
Jaguar	86.8	89.9	88.1
Tiger	89.8	90.1	86.5
Lion	98.3	90.6	90.6
Leopard	90.5	94.8	86.2
Puma	89.5	99.6	81.0
Clouded leopard	83.7	99.7	82.7
Snow leopard	94.6	105.0	84.7
Cheetah	103.3	105.0	87.1
M. parvulus	94.9	100.2	80.5

Extant felid species are not strictly confined to one specific habitat. However, their limb proportions reflect their preferred habitat and locomotor style. Limb proportions have also been used to infer the habitat preferences of extinct species (Gonyea, 1976a, 1976b; Lewis, 1997; Werdelin and Lewis, 2001). Carnivorans and more specifically felids that inhabit relatively open environments are generally more cursorial and have more elongated distal segments than felids adapted to mixed or closed habitats. The humeroradial index has been used as a general indicator of habitat preference and cursoriality. Species inhabiting open habitats tend to have a greater humeroradial index. The cheetah, which is the fastest felid and inhabits open environments almost exclusively, has the largest humeroradial index, and is the only large felid with a radius that is longer than the humerus (Gonyea, 1976a). The radius of the lion is also relatively elongated, but is shorter than the humerus. In *M. parvulus*, the radius is relatively shorter than in the cheetah and the lion, but longer than in the jaguar and the clouded leopard, which seem to prefer relatively more highly structured environments. The humeroradial index of *M. parvulus* is comparable (Table 22) to that of the snow leopard, a felid that inhabits open woodlands on the slopes of the mountains (Gonyea, 1976a). Regarding the posterior limb, the tibia of *M. parvulus* is relatively large, and the femorotibial index is almost the same with that of the puma and the clouded leopard (Table 22). *M. parvulus* has an elongated posterior limb relative to the anterior one. This is reflected in its low intermembral index, which is comparable to that of the puma (Table 22). A long posterior limb relative to the anterior one is generally considered an indication of jumping skills (Howell, 1944; Ballesio, 1963; Gonyea, 1976a). A long posterior limb relative to the anterior limb also characterises extant lynxes, which are excellent leapers. According to the data provided by Kurtén (1978) and following his methodology, the intermembral index of *L. lynx* is almost the same with that of the puma and *M. parvulus*. However, in *L. lynx* the humerus contributes to the total length of the anterior limb almost as much as the radius, while in *M. parvulus* and the puma the contribution of the humerus is

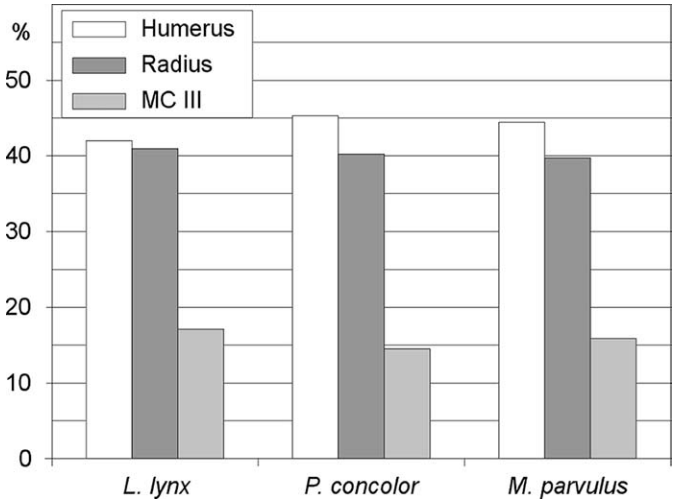

Fig. 11. Relative lengths of the limb-bone elements of the anterior limb. Total length of the anterior limb = 100. (Methodology, and data for *L. lynx* and *P. concolor* according to Kurtén (1978)).
Fig. 11. Diagramme graphique des longueurs relatives des segments du membre antérieur. Longueur totale du membre antérieur = 100.

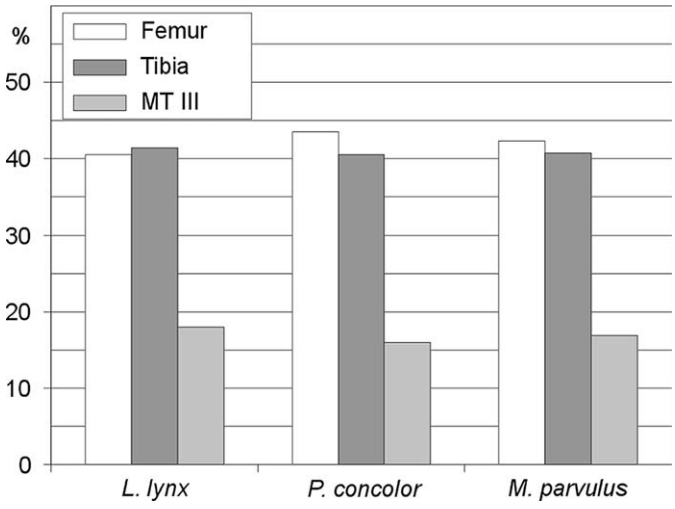

Fig. 12. Relative lengths of the limb-bone elements of the posterior limb. Total length of the posterior limb = 100. (Methodology, and data for *L. lynx* and *P. concolor* according to Kurtén (1978)).
Fig. 12. Diagramme graphique des longueurs relatives des segments du membre postérieur. Longueur totale du membre postérieur = 100.

more significant. Concerning the posterior limb the differences are not so important, but again the femur is larger than the tibia both in *M. parvulus* and the puma, unlike *L. lynx*. The relative contribution of the metapodials to the limb lengths in *M. parvulus* is larger than in the puma but smaller than in *L. lynx* (Figs. 11 and 12).

5. Discussion

The species *Metailurus parvulus* (Hensel, 1862) was originally based on specimens from Pikermi described as *Machairodus parvulus*, and also includes *Felis leiodon* Weithofer, 1888 (Thenius, 1951; Beaumont, 1961). Dental remains attributed to *M. parvulus* are known from various Turolian localities of Europe, such as Pikermi, Halmyropotamos and Chomateri in Greece (Hensel, 1862; Thenius, 1951; Melentis, 1968; Symeonidis, 1978), and Los Mansuetos and El Arquillo in Spain (Morales and Soria, 1979; Fraile et al., 1997). Outside Europe, a mandible from Maragha described by Kittl (1887) as *Felis* cf. *brevirostris* belongs to *M. parvulus* according to Beaumont (1961). Moreover, according to Thenius (1951) and Beaumont (1961), *M. parvulus* also includes the species *Metailurus minor* Zdansky, 1924, which was based on specimens from China, a view also adopted here.

A comparison between the Greek and the Chinese specimens attributed to *M. parvulus* shows that the indices of the teeth and the dimensions of the M_1 do not differ, but the lower canine and the premolars tend to have slightly smaller dimensions in the Greek specimens (Table 1 and Fig. 13). The P_4 of *Felis* cf. *brevirostris* from Maragha (Kittl, 1887), which according to Beaumont (1961) belongs to *M. parvulus*, and the P_4 from Los Mansuetos (Morales and Soria, 1979) are also slightly smaller than the Chinese specimens. Nevertheless, these differences are not significant. Observations that concern the postcanine diastema and its relative length might be considered of greater importance. The Greek *M. parvulus* specimens tend to have slightly larger diastemata relative to the P_3 ($C_i - P_3/LP_3$) and the cheek teeth ($C_i - P_3/LP_3 + LP_4 + LM_1$) than the Chinese specimens (Table 1). Possible differences in the length of the diastema relative to the carnassial ($C_i - P_3/LM_1$) are not clearly indicated, because both Zdansky (1924) and Thenius (1951) provided measurements for Chinese and Greek specimens that lacked the P_3. The diastema could vary significantly, exhibiting sexual dimorphism, as is the case in some extant felids (Rothwell, 2003). However, our comparison is based on a limited number of specimens and on data collected from various bibliographic sources. Therefore, the above observations indicate that further comparison between the Greek and the Chinese specimens attributed to *M. parvulus* is required, using standardized methodology.

Although felid dental remains are well represented in late Miocene localities, limb-bones are rare, and associated limb-bones are even rarer. Some described limb-bones come mainly from the Turolian locality of Pikermi. Kovatchev (2001) described an almost complete skeleton from Hadjidimovo-1 (Girizite) in Bulgaria and referred this to a new species of *Metailurus*: *Metailurus anceps.* However, this skeleton is referred to *Metailurus* cf. *major* by Spassov (2002).

A distal radius fragment from Pikermi (MNHNP PIK3128), described by Gaudry (1862–1867: Pl. 17, Fig. 8) as "*Felis* 3ème espèce", is very similar in dimensions and morphology to the Kerassia 1 radius (Table 9). This specimen must be attributed to *M. parvulus*, as has previously been suggested by various authors (Thenius, 1951; Beaumont, 1961; Roussiakis, 2002).

The radius from Pikermi (MNHNP PIK3258) referred to "*Felis* 2ème espèce" by Gaudry (1862–1867: Pl. 17, Fig. 4) is much larger than the *M. parvulus* radius from Kerassia 1, and cannot belong to this species. This specimen appears comparable in dimensions to the "*M. anceps*" radius from Hadjidimovo-1 (Table 9).

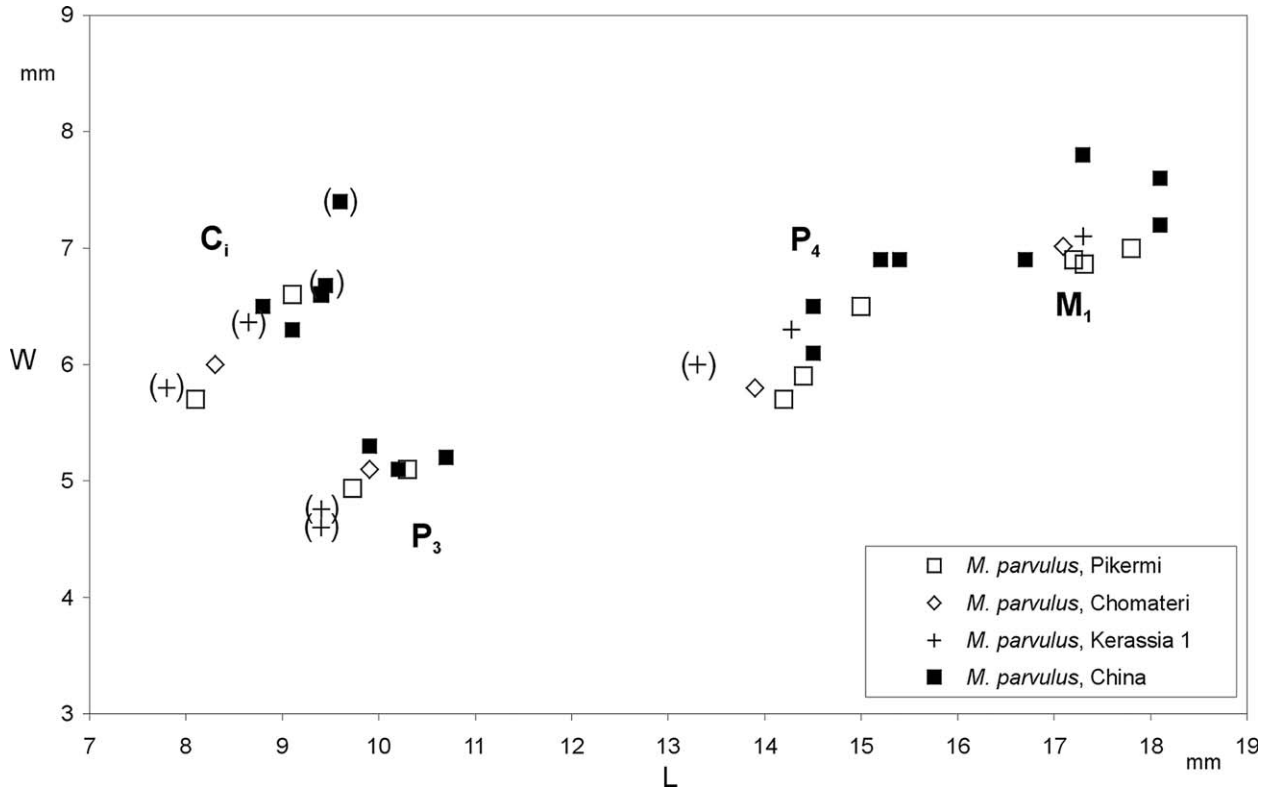

Fig. 13. Bivariate scatter diagram of the teeth of *M. parvulus* from different localities.
Fig. 13. Diagramme de dispersion des dents de *M. parvulus* des localités différentes.

Some dental and postcranial specimens from Pikermi described as "*Machairodus schlosseri*" by Weithofer (1888: Pl. 11, Figs. 1–7) have been subsequently attributed to *Paramachairodus orientalis* (Kittl, 1887) by some authors (Pilgrim, 1931). Among these specimens there is a radius with length estimated to 184 mm (based on Weithofer's figure). Another radius of comparable length is NHML M9006 from Pikermi referred to by Pilgrim (1931) to *P. orientalis*. These two radii possibly belong to the same species, and appear intermediate in length between the Kerassia 1 and the "*Felis* 2ème espèce" radii (Table 9). Judging from the size variation of extant felids, these specimens could represent large individuals of *M. parvulus*. The "*M. schlosseri*" radius, however, differs from the *M. parvulus* radius from Kerassia 1 in some details, such as the position of the distal tip of the radius relative to the medial margin of the shaft, whereas in this character it resembles the radius NHML M9006. Pilgrim (1931) also attributed a humerus from Pikermi (NHML M8960) to *P. orientalis*. This humerus is comparable in length to the "*M. anceps*" humerus, but it is large relative to the radius M9006 or the "*M. schlosseri*" radius (Table 7). The metacarpals of "*M. schlosseri*" (Weithofer, 1888: Pl. 11, Fig. 2) are slightly larger than those of *M. parvulus* from Kerassia 1 (Table 12).

A distal half of a tibia (MNHNP PIK3255) and some tarsal and metatarsal bones (MNHNP PIK3041) described by Gaudry (1862–1867: Pl. 17, Figs. 2 and 3) as "*Felis* 1ème espèce" as well as the calcaneus MNHNP PIK3286 are larger than the corresponding bones of *M. parvulus* from Kerassia 1, and are generally comparable in dimensions to "*M. anceps*" (Tables 15–20).

A tibia from Pikermi (MNHNP PIK3256), referred to by Gaudry (1862–1867: Pl. 17, Fig. 7) as "*Felis* 2ème espèce", is slightly longer than the *M. parvulus* tibia from Kerassia 1, and slightly more slender. These differences are very small. Nevertheless, there are some morphological differences, as the medial malaeolus of PIK3256 appears more vertical, and is projected further distally than in *M. parvulus* from Kerassia 1. The correlation of this specimen with others is difficult, but it could belong to the same species as the radius M9006 and the "*M. schlosseri*" radius described by Weithofer.

Concerning all these postcranial elements it is very difficult to reach unambiguous conclusions, since felids show important intraspecific size variation. Moreover, the limb proportions and the proportions between the various limb segments can vary in different species, which makes it difficult to associate the limb bones if no data is available as to whether these were found articulated or not.

From the above comparisons, however, we provisionally attribute the radius MNHNP PIK3258 ("*Felis* 2ème espèce"), the tibia MNHNP PIK3255 ("*Felis* 1ème espèce"), the tarsal and metatarsal bones MNHNP PIK3041 ("*Felis* 1ème espèce"), the calcaneum MNHNP PIK3286, and the humerus NHML M8960, to the same species, probably *M. major*. Their dimensions are comparable to those of "*M. anceps*". The radius

NHML M9006, and the "*M. schlosseri*" specimens described by Weithofer (1888) could belong to the same species, probably *P. orientalis*. The tibia MNHNP PIK3256 ("*Felis* 2ème espèce") could also belong to the same species.

6. Palaeoecology

Since the excavations of the K1 site are still in progress, the collected material is still inadequate, and each taxon is represented by a relatively small number of specimens. Therefore, it is not possible to define the dominant taxa, which could provide indications about the prevailing character of the palaeoenvironment. However, the available faunal data indicate that the K1 site possibly represented a landscape with a mosaic of biotopes. Such an environment could provide various ecological niches, with grasslands that supported grazer species, and woodland vegetation that supported browsers. Taxa such as *Gazella* sp. and probably *Samotherium major* might have inhabited relatively open areas, whereas *Helladotherium duvernoyi* and *Microstonyx major erymanthius* probably frequented areas with denser vegetation. *Palaeotragus rouenii* is considered a mixed feeder (Solounias et al., 2000), *Tragoportax amalthea* an inhabitant of lightly wooded country (Gentry et al., 1999), while the preferable habit of the *Orycteropus* sp. could be an open grassland landscape, but extant *Orycteropus* also occurs in forests (Patterson, 1975).

Recently, Iliopoulos (2003) studied the histological and biogeochemical alterations of the fossil bones and teeth from the Kerassia sites. He identified extensive microscopical focal destruction (Hackett, 1981) in all examined specimens from the bone-bearing bed of K1, and concluded that a seasonal, warmer and relatively wetter climate than today's Mediterranean can be inferred for the late Miocene of Kerassia.

The humeroradial index of *M. parvulus* indicates that this species did not have the extreme cursorial abilities of the cheetah, and was not adapted to high-speed sprinting in open areas. However, it was more cursorial than closed or closed/mixed habitat species, such as the clouded leopard, jaguar and tiger. Extant felids may frequent more than one habitat. This could also be the case with *M. parvulus*, given that it does not seem to be a specialised inhabitant of exclusively open or closed areas. However, the humeroradial index of *M. parvulus* indicates that this species had moderately developed cursorial adaptations, and probably frequented primarily more open woodlands than species that prefer relatively closed habitats. The posterior limb of *M. parvulus* is elongated relative to the anterior one, as is shown by its large intermembral index, which reflects great jumping skills. *Metailurus parvulus* could pounce on small prey, but its body weight, about 40 kg, indicates that it might also feed on larger prey of comparable body weight (Carbone et al., 1999), as gazelles and small sized antelopes. In such cases, *M. parvulus* could occasionally stalk its prey and leap upon the victim's back after a short distance rush. Climbing trees cannot be excluded, and could be facilitated by its jumping abilities. Nevertheless, our data do not support an arboreal mode of life.

7. Conclusions

The almost complete skeleton of *M. parvulus* found in the Kerassia 1 site gave us the opportunity to describe its skeleton, compare it with already described limb-bone elements from Pikermi, and draw some conclusions concerning the habitat preferences and cursorial adaptations of this species. Also, a proximal humerus fragment from the site of Kerassia 4 can provisionally be attributed to *M. parvulus*. The Kerassia 4 site belongs to the lower fossiliferous level, which stratigraphically is relatively older than the site of Kerassia 1.

Comparison of the available dental material indicates that there are no differences between the Kerassia 1 specimens and those of Pikermi and Chomateri. Following Thenius (1951) and Beaumont (1961), *M. minor* from China is considered a synonym of *M. parvulus*. The specimens from Kerassia 1, Pikermi and Chomateri do not differ significantly in size from the specimens from China. It has been observed, however, that the specimens from China probably have slightly smaller diastemata relative to the cheek teeth length, which suggests that the synonymy of *M. minor* with *M. parvulus* is not clear.

The available palaeocological data for the Kerassia 1 site indicate that the landscape was a mosaic of relatively open areas with grasslands and areas covered in wood vegetation. The described material indicates that *M. parvulus* was a medium sized felid, with moderately developed cursorial adaptations, which probably frequented lightly wooded areas, but not exclusively so. Its posterior limb was elongated relative to the anterior one, as is shown by its large intermembral index, which reflects great jumping skills.

Acknowledgments

We thank Professor Dr. E. Velitzelos (University of Athens) for providing us with information concerning the existence of fossil mammals close to the Kerassia village, Northern Euboea. Since 1992, the excavations have been financed by the University of Athens Research Account (Project 70/4/1397), the Municipality of Nileas and the Local Council of Northern Euboea (Project 70/3/2842), and the General Secretary of Research and Technology (Project 95ΣΥΝ107, 70/3/3922). We are grateful to Dr. J. Hooker (Natural History Museum of London) and Dr. L. Ginsburg (Muséum national d'Histoire naturelle de Paris) who granted us access to the respective museum collections. The authors are also indebted to Dr. L. Werdelin (Senior Curator, Swedish Museum of Natural History, Department of Palaeozoology) and Professor Dr. L. de Bonis (Laboratoire de Géobiologie, Biochronologie et Paléontologie Humaine CNRS UMR 6046, Université de Poitiers) for their useful comments and suggestions on the manuscript.

References

Andersson, K., 2004. Predicting body mass from a weight-bearing joint. Journal of Zoology 262, 161–172.

Antón, M., Galobart, À., 1999. Neck function and predatory behavior in the scimitar toothed cat *Homotherium latidens* (Owen). Journal of Vertebrate Paleontology 19, 771–784.

Anyonge, W., 1993. Body mass in large extant and extinct carnivores. Journal of Zoology 231, 339–350.
Ballesio, R., 1963. Monographie d'un Machairodus du gisement Villafranchien de Senèze: *Homotherium crenatidens* Fabrini. Travaux du Laboratoire de Géologie de la Faculté des Sciences de Lyon 9, 1–129.
Beaumont, G. de, 1961. Recherches sur *Felis attica* Wagner du Pontien eurasiatique avec quelques observations sur les genres *Pseudaelurus* Gervais et *Proailurus* Filhol. Nouvelles Archives du Muséum d'Histoire Naturelle de Lyon 6, 1–45.
Beaumont, G. de, 1986. La patte postérieure de *Felis attica* Wagner (Mammifère, Carnivore) du Turolien de Grèce. Archives des Sciences 39, 377–386.
Behrensmeyer, A.K., 1978. Taphonomic and ecologic information from bone weathering. Paleobiology 4, 150–162.
Bryant, H.N., Russell, A.P., Laroiya, R., Powell, G.L., 1996. Claw retraction and protraction in the Carnivora: skeletal microvariation in the phalanges of the Felidae. Journal of Morphology 229, 289–308.
Carbone, C., Mace, Craig Roberts, S., Macdonald, D.W., 1999. Energetic constraints on the diet of terrestrial carnivores. Nature 402, 286–288.
Christiansen, P., 1999. Scaling of mammalian long bones: small and large mammals compared. Journal of Zoology 247, 333–348.
Egi, N., 2001. Body mass estimates in extinct mammals from limb bone dimensions: the case of North American Hyaenodontids. Palaeontology 44, 497–528.
Evans, H.E., Christensen, G.C., 1979. Miller's Anatomy of the Dog. W.B. Saunders Company, Philadelphia.
Fraile, S., Pérez, B., de Miguel, I., Morales, J., 1997. Revisión de los carnívoros presentes en los yacimientos del Neógeno español. In: Calvo, J.P., Morales, J. (Eds.), Avances en el conocimiento del Terciario Ibérico. III Congresso del G.E.T., Cuenca, pp. 77–80.
Galobart, À., Pons-Moyà, J., Antón, M., Maroto, J., 2003. Descripción del material de *Homotherium latidens* (Owen) de los yacimientos del Pleistoceno inferior de Incarcal (Girona, NE de la Península Ibérica). Paleontologia i Evolució 34, 99–141.
Gaudry, A., 1862–1867. Animaux fossiles et géologie de l'Attique. F. Savy, Paris.
Gentry, A.W., Rössner, G.E., Heizmann, E.P.J., 1999. Suborder Ruminantia. In: Rössner, G.E., Heissig, K. (Eds.), The Miocene Land Mammals of Europe. Pfeil, München, pp. 225–258.
Gonyea, W.J., 1976a. Adaptive differences in the body proportions of large felids. Acta Anatomica 96, 81–96.
Gonyea, W.J., 1976b. Behavioral implications of saber-toothed felid morphology. Paleobiology 2, 332–342.
Hackett, C.J., 1981. Microscopical focal destruction (tunnels) in exhumed Human bones. Medicine, Science and the Law 21, 243–265.
Hensel, R.F., 1862. Über die Reste einiger Säugetierarten von Pikermi in der Münchener Sammlung. Monatsberichte der Akademie der Wissenschaften 27, 560–569.
Hildebrand, M., 1952. An analysis of body proportions in the Canidae. American Journal of Anatomy 90, 217–256.
Hopwood, A.T., 1945. Contributions to the study of some African mammals. III. Adaptations in the bones of the fore-limb of the lion, leopard, and cheetah. Journal of the Linnean Society (Zoology) 41, 259–271.
Howell, A.B., 1944. Speed in Animals. University of Chicago Press, Chicago.
Iliopoulos, G., 2003. The Giraffidae (Mammalia, Artiodactyla) and the study of histology and chemistry of fossil mammal bone from the Late Miocene of Kerassia (Euboea Island, Greece). Ph.D Thesis, Department of Geology, University of Leicester (unpublished).
Jayne, H., 1898. Mammalian Anatomy, a Preparation for Human and Comparative Anatomy. Part 1. The Skeleton of the Cat. J.B. Lippincott Company, London.
Kittl, E., 1887. Beiträge zur Kenntiss der fossilen Säugetiere von Maragha in Persia. I. Carnivoren. Annalen des Kaiserlich-königlichen Naturhistorischen Hofmuseums 2, 317–338.
Kovatchev, D.B., 2001. Description d'un squelette complet de *Metailurus* (Felidae, Carnivora, Mammalia) du Miocène supérieur de Bulgarie. Geologica Balcanica 31, 71–88.
Kurtén, B., 1978. The lynx from Etouaries, *Lynx issiodorensis* (Croizet and Jobert), late Pliocene. Annales Zoologi Fennici 15, 314–322.
Legendre, S., Roth, C., 1988. Correlation of carnassial tooth size and body weight in recent carnivores (Mammalia). Historical Biology 1, 85–98.
Lessertisseur, J., Saban, R., 1967. Squelette axial. In: Grassé, P.P. (Ed.), Traité de Zoologie, Anatomie, Systématique, Biologie, tome 16, fascicule 1, Mammifères, Téguments et Squelette. Masson et Cie, Paris, pp. 584–708.
Lewis, M.E., 1997. Carnivoran paleoguilds of Africa: implications for hominid food procurement strategies. Journal of Human Evolution 32, 257–288.
Melentis, J.K., 1968. Studien über fossile Vertebraten Griechenlands. 19. Die Pikermifauna von Halmyropotamos (Euböa—Griechenland). 1. Teil: Odontologie und Kraniologie. Annales Géologiques des Pays Helléniques 19, 285–411.
Morales, J., Soria, D., 1979. Nuevos datos sobre los carnívoros del área de Teruel. Síntesis y bioestratigrafía. Estudios Geológicos 35, 497–504.
Patterson, B., 1975. The fossil aardvarks (Mammalia: Tubulidentata). Bulletin of the Museum of Comparative Zoology 147, 185–236.
Pilgrim, G.E., 1931. Catalogue of the Pontian Carnivora of Europe in the Department of Geology. Museum (Natural History), London 1–174.
Rawn-Schatzinger, V., 1992. The scimitar cat *Homotherium serum* Cope. Osteology, functional morphology, and predatory behavior. Contributions to Geology, University of Wyoming, Reports of Investigations, Illinois State Museum 47, 1–80.
Reighard, J., Jennings, H.S., 1901. Anatomy of the Cat. Henry Holt and Company, New York.
Rothwell, T., 2003. Phylogenetic systematics of North American *Pseudaelurus* (Carnivora, Felidae). American Museum Novitates 3403, 1–64.
Roussiakis, S.J., 2002. Musteloids and feloids (Mammalia, Carnivora) from the late Miocene locality of Pikermi (Attica, Greece). Geobios 35, 699–719.
Roussiakis, S.J., Theodorou, G.E., 2003. Carnivora from the Late Miocene of Kerassia (Northern Euboea, Greece). Deinsea 10, 469–497.
Russell, A.P., Bryant, H.N., 2001. Claw retraction and protraction in the Carnivora: the cheetah (*Acinonyx jubatus*) as an atypical felid. Journal of Zoology 254, 67–76.
Smith, J.R., 1993. Bias in equations used to estimate fossil primate body mass. Journal of Human Evolution 25, 31–41.
Solounias, N., McGraw, W.S., Hayek, L.A., Werdelin, L., 2000. The paleodiet of Giraffidae. In: Vrba, E.S., Schaller, G.B. (Eds.), Antelopes, Deer, and Relatives: Fossil Record, Behavioral Ecology, Systematics and Conservation. Yale University Press, New Haven and London, pp. 84–95.
Spassov, N., 2002. The Turolian Megafauna of West Bulgaria and the character of the Late Miocene "Pikermian biome". Bolletino della Società Paleontologica Italiana 41, 69–81.
Symeonidis, N.K., 1978. Ein Schädel von *Metailurus parvulus* (Hensel) aus Pikermi (Attica, Griechenland). Annales Géologiques des Pays Helléniques 29, 698–703.
Thenius, E., 1951. Zur odontologischen Charakteristik von "*Felis*" *leiodon* aus Pikermi (Griechenland). Neue Jahrbuch für Geologie und Paläontologie (3), 88–96.
Theodorou, G.E., Athanassiou, A., Iliopoulos, G., Roussiakis, S.J., 2004. Remarks on the Late Miocene vertebrates of Kerassia (Northern Euboea, Greece). Distribution and Migration of Tertiary Mammals in Eurasia. University of Utrecht, 17–19 May Abstracts, pp. 44-45.
Theodorou, G.E., Athanassiou, A., Roussiakis, S.J., Iliopoulos, G., 2003. Preliminary remarks on the Late Miocene herbivores of Kerassiá (Northern Euboea, Greece). Deinsea 10, 519–530.
Van Valkenburgh, B., 1990. Skeletal and dental predictors of body mass in carnivores. In: Damuth, J., Macfadden, B.J. (Eds.), Body Size in Mammalian Paleobiology. Cambridge University Press, Cambridge, pp. 181–205.
Van Valkenburgh, B., Grady, F., Kurtén, B., 1990. The Plio-pleistocene cheetah-like cat *Miracinonyx inexpectatus* of North America. Journal of Vertebrate Paleontology 10, 434–454.
Weithofer, A., 1888. Beiträge zur Kenntniss der Fauna von Pikermi bei Athen. Beiträge zur Paläontologie Oesterreich-Ungarns 6, 225–292.
Werdelin, L., Lewis, M.E., 2001. A revision of the genus *Dinofelis* (Mammalia, Felidae). Zoological Journal of the Linnean Society 132, 147–258.
Werdelin, L., Solounias, N., 1991. The Hyaenidae: taxonomy, systematics and evolution. Fossils and Strata 30, 1–105.
Zdansky, O., 1924. Jungtertiäre Carnivoren Chinas. Palaeontologia Sinica 2, 1–149.